Determination of Phase Characteristics for PVDF Membrane Hydrophones in the Frequency Range 1-100 MHz using Nonlinear Acoustics Approach

A Thesis Submitted to the

Faculty

of Drexel University

by

Gaurav Gandhi

In partial fulfillment of the

requirements for the degree of

Master of Science

March 2009

Dedication

To My Family

Acknowledgement

First and foremost, I would like to thank my advisor Dr. Peter A Lewin. This study would not have been possible without his constant support and encouragement. His pertinent knowledge and analysis of the problem helped me to understand the basic and advanced topics of acoustics.

I would like to thank Dr. Philip Bloomfield for his contributions to our understanding of the nonlinear model. His deep understanding of the nonlinear acoustics and instrumentation helped me at every step of the project.

I sincerely thank Dr. Afshin Daryoush for, his guidance on the Fiber Optic hydrophone and being in my defense committee. His support and encouragement are highly appreciated.

I would also like to thank the School of Biomedical Engineering, Science and Health System for their constant support. The faculty and staff of the school helped me through difficult and demanding times.

The phase characterization study was also partly supported by the National Institute of Health (NIH grant #5 ROI EB007117-02).

I wish to thank Dr. Sumet Umchid for introducing me to the world of acoustics; Piyush Arora for his comments and guidance regarding nonlinear measurements and life in general; Rupa Gopinath and Khushali Manseta for their inputs on the Fiber Optic hydrophone.

I would also like to thank Sakya Sing Mohapatra, Sandip Banerjee, Sameet Shreyan, Kalyan Chakravarthy, Oluseeni Komolafe, Shankar Narayan, Prasanna, Vamsi, Sidharth Gadkari, Vishal Kamat, Arun Hotra Ganti, Aanchal Malik, Anant Shayanam and all my friends in India and US for their everlasting support and words of wisdom.

I would like to take this opportunity to thank my Grandparents, Uncles, Aunts, and Cousins for their love and encouragement throughout my life.

Last but not the least; I thank my Father, Mother, Sister and the Almighty, from the bottom of my heart for being the guiding light in my life.

Contents

List of Figures vi

Abstract x

Chapter 1: Introduction 1

Chapter 2: Background and Significance 3

2.1 Significance 3

2.2 Hydrophone probes used in phase measurements 7

2.3 Nonlinear wave propagation and the JW model 13

2.4 Normalized pressure-time signal 19

2.5 Surface apodization function 21

Chapter 3: Methodology 22

3.1 Acoustic source pressure-time waveform measurements 22

3.2 Acoustic source characterization 26

3.3 Nonlinear Field Simulation 31

3.4 Evaluation of the Phase response 33

3.5 Hydrophone Simulation PiezoCAD software 34

Chapter: 4 Results 36

Chapter: 5 Discussion and Conclusions 52

References 56

APPENDIX I 59

APPENDIX II Assessment of overall uncertainty of hydrophone calibration system 60

List of Figures

	Title	pp.
Figure 2.1	Flow diagram of the nonlinear approach to find phase characteristics	6
Figure 2.2	Bilaminar membrane hydrophone (Sonora Medical Systems, Longmont-Colorado)	8
Figure 2.3	Photograph of a needle PVDF hydrophone and (b) the details of the sensor element	10
Figure 2.4	Schematic representation of the line capacitance effects on end-of-cable sensitivity. Ca, Cc, Cs are the hydrophone element, coaxial cable, and stray capacitances respectively. Mc and ML are end of the cable loaded and end of cable sensitivities respectively	12
Figure 2.5	Normalized pressure-time waveform generated by JW nonlinear model, used as input for simulation of burst with of 10 cycles, 5 MHz center frequency, $E_{windows}$ of 20. The Y axis is the normalized acoustic pressure and the X axis is the retarded time normalized to 2π	20
Figure 2.6	Spectrum pulse of the normalized pressure-time waveform modeled with the parameters of fundamental frequency: 5 MHz, 10 cycles and envelope coefficient of 20	20
Figure 3.1	Experimental setup for acquisition of nonlinear pressure-time acoustic waveform using an acoustic source and a hydrophone in the focal plane	23
Figure 3.2	Phase response of the Preamplifier SEA 377	25
Figure 3.3	Comparison between the calculated normalized apodization function and the one obtained through the measurements performed at 10 mm axial distance from the surface of the 5MHz acoustic transducer	27
Figure 3.4	Contour plot of the isobars generated by 5 MHz HIFU transducer. The plot was obtained using needle hydrophone at the focal plane (35 mm axial distance from the transducer's surface)	28
Figure 3.5	Color representation of data shown in Figure3.4	28
Figure 3.6	3-D reconstruction of the isobar shown in Figure 3.5	29
Figure 3.7	Comparison between the normalized experimental and simulated pressure-time waveform. The measurement was performed near the surface (3 mm) of the 5 MHz focal number HIFU acoustic source by the 150μm diameter needle hydrophone	29

Figure 3.8	1-D scan along the acoustic axis at low pressure amplitude corresponding to 0.013 MPa, to find the focal distance of the 1.52 MHz HIFU source used in the study by a needle hydrophone	30
Figure 3.9	Flow diagram of the steps involved to run the JW simulation	32
Figure 4.1	Pressure-time waveform recorded by the needle hydrophone (see Chapter 3) at the surface of the HIFU source operating at 5 MHz, 134 Vpp, and 4 cycles tone burst	37
Figure 4.2	FFT of the pressure time waveform recorded at the surface of 1.52 MHz HIFU source. It confirms absence of harmonics at the maximum excitation voltage applied to the terminals of the HIFU source	38
Figure 4.3	Pressure distribution along the acoustic axis, as estimated by the nonlinear JW model for 1.52 HIFU source excited by 10 cycles at 134 Vpp: Fundamental (5MHz) (Solid red line), Second harmonic (blue dotted lines), Third harmonic (green dashed line), Fourth harmonic (dashed dotted pink lines)	38
Figure 4.4	Amplitude sensitivity obtained by TDS method, of the Marconi hydrophone used in our study up to 40 MHz	39
Figure 4.5	Nonlinear pressure-time waveform as measured by the Marconi Membrane Hydrophone and generated by the 1.52 MHz HIFU operating at its third harmonic of 5 MHz with excitation voltage of 134 Vpp	40
Figure 4.6	Scaled nonlinear pressure-time waveform as simulated by the JW model, corresponding to the input parameters: Surface Pressure 1.5 MPa and frequency of 5 MHz	41
Figure 4.7	Amplitude of the FFT response of the experimentally measured pressure-time waveform of Fig. 4.5	41
Figure 4.8	Amplitude of the FFT response of the experimentally measured pressure-time waveform Fig.4.5, (yellow solid lines), and the amplitude response of the complex field generated by the JW model (red solid lines	42
Figure 4.9	Relative phase response of the complex field generated by the nonlinear model and shifted with respect to the phase at fundamental frequency, i.e. 5 MHz corresponding to Fig. 4.6	43
Figure 4.10	Relative phase response of the complex field measured by the Marconi hydrophone and shifted with respect to the phase at the fundamental frequency of the HIFU source; i.e. 5 MHz corresponding to Fig. 4.5	43
Figure 4.11	Final result of the Phase calibration for 50μm thick Marconi bilaminar membrane hydrophone, effective diameter - 500μm, cable length of 65 cm	44
Figure 4.12	Amplitude Calibration of a similar Marconi hydrophone calculated by using nonlinear approach	45

Figure 4.13	Final phase shift for 500μm effective diameter Marconi hydrophone with 50μm thick PVDF membrane and terminated by a 65 cm coaxial cable is given by red crosses, and the PiezoCAD relative phase results are given by blue crosses. Pressure-time waveform is generated by a 5 MHz HIFU source. The calibration is based on the result predicted by JW model	47
Figure 4.14	Pressure-time waveform measured by Precision Acoustics membrane hydrophone with an effective diameter of 400μm, 10 cycles and generated by a 10 MHz frequency HIFU source excited by a 10 cycle pulse of 150 Vpp level	48
Figure 4.15	Normalized amplitude response of the pressure-time waveform depicted in Fig. 4.14	48
Figure 4.16	Relative phase response of the pressure-time waveform in Fig. 4.14	49
Figure 4.17	Normalized amplitude response of the complex field generated by the JW model for the 10 MHz HIFU source	49
Figure 4.18	Relative phase simulated by JW model for the 10 MHz source	50
Figure 4.19	Final phase shift for 400μm effective diameter Precision Acoustics hydrophone terminated by a 1.3 cm coaxial cable and a 20 dB preamplifier, calculated using Eqs (22)-(24)	50
Figure 4.20	Amplitude calibration of the 400μm effective diameter Precision Acoustics membrane hydrophone terminated by a 1.3 meter coaxial cable and a 20 dB ONDA preamplifier	51

Abstract

Determination of Phase Characteristics for PVDF Membrane Hydrophones in the Frequency Range 1-100 MHz using Nonlinear Acoustics Approach

Gaurav Gandhi
Peter A. Lewin, Ph.D.

The purpose of this study was to verify and refine a phase calibration technique reported last year, based on the nonlinear acoustic wave propagation in water. The nonlinearity of the medium leads to the generation of harmonics and the relative phasing of the harmonics causes a distinct asymmetry between the positive and negative pressure levels affecting the rise and fall time of the examined waveforms. Knowledge of the relative phase shift measured in terms of radians versus frequency when referenced to the uniform simulated phase can help deconvolve the pressure-time signal, and hence produce its faithful reconstruction, including the rise times and peak amplitudes. The modified scheme discussed in this dissertation, uses an advanced semi-empirical computer model which predicts the near and the far field distributions using the hyperbolic propagation operator, in contrast to the parabolic approximations used elsewhere. Two PVDF membrane hydrophones were first calibrated in terms of their amplitude sensitivity in Volts/Pascals or dB re 1V/μPa. The sensitivities were needed to calculate the pressure levels generated by the HIFU (High Intensity Focused Ultrasound) sources. The sources operated at the frequencies of 5 MHz and 10 MHz to enable studies up to 100 MHz. The phase responses of these two hydrophones - a Marconi 50μm thick, 500μm diameter bilaminar PVDF film membrane hydrophone and a custom made Precision Acoustics, 9μm thick, 400μm diameter hydrophone - were determined with

respect to the relative phase extracted from the complex frequency response of the nonlinear field simulated by the advanced semi-empirical hyperbolic operator model. The results indicate that the nonlinear technique is primarily suited for membrane hydrophones having a flat frequency response with variation in the range of ±10 %. Another PVDF hydrophone probe design, namely the needle one, does not exhibit uniform frequency response due to intrinsic (radial mode) resonances. These resonances introduce electrical distortions in the measured signals, which complicate the separation of the medium generated harmonics and those produced at the hydrophone output. Therefore, in order to calibrate the needle probes, a fiber optic hydrophone with a flat frequency response and zero phase-shift in the frequency range considered would be preferable. The main limitation of the nonlinear approach to determine phase response of membrane hydrophones is caused by the fact the technique can only provide phase information at discrete frequencies which are multiples of the fundamental of the acoustic source. Another limitation is associated with the use of preamplifier. No preamplifier and hence no electrical impedance matching was used to measure high pressure levels above 4 MPa (corresponding to the HIFU sources excitation levels of about 100Vpp), because of the observed saturation (clipping) of the electrical signal. This clipping reduced the number of harmonics which could be measured, and effectively limited the calibration bandwidth. The uncertainties of the measurements were analyzed and are presented at 95% confidence levels.

In conclusion, we have demonstrated that the nonlinear acoustic wave propagation can be used as an effective tool to determine complex frequency response of the ultrasound PVDF membrane hydrophones in frequency range of 1-100 MHz.

.

Chapter 1: Introduction

This thesis is based on various aspects of acoustics measurements, ultrasonic field simulations for a wide variety of HIFU transducers, and membrane and needle hydrophones acting as receivers.

The specific aim of this project was to verify and refine a phase characterization technique for membrane hydrophones, with the amplitude and the phase components of the experimental data compared with the nonlinear simulations acting as reference, in the frequency range up to 100 MHz. Knowledge of the relative phase shift measured in terms of radians versus frequency when referenced to the uniform simulated phase will allow deconvolution of the pressure-time signal, and hence produce its faithful reconstruction, including the rise times and peak amplitudes. The finite amplitude model used in the study approximately solves the hyperbolic equations for a circularly focused acoustic source. The phase shifts were verified by comparing to the phase generated by the commercially available PiezoCAD software. The simulations were experimentally verified for membrane and needle hydrophones in the desired frequency range, placed in a non-linear field generated by a HIFU transducer with fundamental frequency of 1.52 MHz, operating at its third harmonic resonance at 5MHz. Two different hydrophones were used to establish broad applicability of the approach.

In Chapter 2 we discuss the background and significance of the project. Chapter 3 explains the procedures and the methodology involved in the study. It also gives an

account of all the instruments used, and protocols followed. Chapter 4 presents the experimental results obtained by this nonlinear method of phase characterization. Chapter 5 discusses and comprehensively interprets the results. It also looks at the future technologies for which the results discussed in this research might become relevant.

Chapter 2: Background and Significance

This chapter emphasizes the background and motivation behind this project; it also describes the tools required to comprehend the results and conclusions discussed in Chapters 4 and 5. Basic principles governing acoustic setup including transducer and hydrophone are presented. A brief explanation of nonlinear acoustics is included to support the understanding of the simulations.

2.1 Significance

Over the last couple of decades ultrasound energy has strengthened its reputation as a safe, reliable and widely used diagnostic and therapeutic technique in the medical world. Use of ultrasound energy does not expose the patient to harmful ionizing radiations and this has helped increase its popularity in the medical community. In addition, it is comforting that the acoustic output of diagnostic ultrasound is limited by FDA regulations [1]. The guidelines specify the limits in terms of different intensities (e.g. Ispta – Intensity Spatial Peak Temporal Average) and MI (Mechanical Index) and TI (Thermal Index) [2-4]. The key acoustic parameter used to determine MI and TI is pressure – time waveform which has to be measured with a calibrated hydrophone. Amplitude calibration gives us the sensitivity ($\frac{Volts}{Pressure}$) of the hydrophone, which is in turn utilized to calculate the pressure being generated by the acoustic transducer when excited at a particular frequency. When the transducer is excited at higher energy levels, the medium's nonlinearity leads to generation of harmonics; hence FDA requires the hydrophone, to be calibrated at least up to 8 times the central frequency of the transducer

being used for imaging or therapeutic purposes [2-4]. In the past decade many new applications of ultrasound technology have been realized, and these frequently use transducers with a wide frequency bandwidth. Currently, ultrasound imaging is being performed in a frequency range of 1-15 MHz with an approximate lateral resolution of 1mm. High frequency ultrasound operating in the frequency range of 30-100 MHz is being used for various purposes which require micrometer resolution [5-7]. Cartilage visualization with penetration depth of 5mm and a microscopic resolution has been investigated at 50 MHz by Kim, et al [5]. Over the years ultrasonic imaging in the frequency range of 40-60 MHz has been developed as an in-vivo and non-invasive technique to image developing mouse embryo [6]. Resolution achievable at 40 MHz is adequate to study the internal structural and the functioning of small animals [7]

As indicated above, for very low frequency imaging systems, operating in the range of 1-2 MHz, the need for calibrating the hydrophone measurement system is only up to a maximum of 20 MHz [8]. But with the invention of advanced imaging transducers and harmonic imaging techniques, transducer arrays operating in the frequency range of 12-15 MHz are being used and calibration techniques up to 100 MHz have been developed [2-4, 9-14].

Another development, which was the basic motivation behind this study, was an increase in the usage of High Intensity Focused Ultrasound (HIFU) [15-17] in the medical field. HIFU is used by the medical professionals as a tool to induce tissue ablation by producing a focused lesion and an elevation of temperature to 55^{o}C and above, by generating I_{SPTA} in a range of 1000 – 10,000 W/cm^2 [18]

There are a number of publications discussing the amplitude calibration techniques for a variety of hydrophones over a wide bandwidth. Substitution techniques are the ones most commonly used worldwide, wherein the amplitude response of the hydrophone under test is compared with a reference hydrophone. The primary calibration can be obtained by interferometric [11, 19], and reciprocity techniques [20, 21]. The finite amplitude approach is used as a reference to provide discrete calibration locations for both linear [22] and nonlinearly distorted fields [10, 11, 23, 24]. Linear frequency sweeps are also used widely to measure the continuous frequency response of the hydrophone [23-27].

A method of amplitude calibration similar to that used in this study, based on the comparison of the experimental data with those simulated by a nonlinear model, was first suggested by Bacon [11, 12]. Baker [13] followed the same principle and assumed plane wave field conditions for his system and hence ignored all spatial averaging corrections. The basic principle for nonlinear calibrating hydrophones using a focused transducer at discrete harmonic frequencies was used by Lum et al. [15, 28], placing the receiver in a harmonic rich nonlinear field. Although this method was used to calibrate a 4μm PVDF membrane hydrophone, the authors advised further work would enable the evaluation of the absolute hydrophone response above 20 MHz [28].

Previous work done regarding the phase calibration technique, which is the main topic of this thesis, is very limited. The corrected phase would help in complete deconvolution of the frequency domain information into reliable pressure-time signal. The most accepted approach proposes to consider a broad band receiver, with a flat amplitude frequency response as a reference and consider the phase response to be flat for the system [29, 30]. The approach examined in this dissertation is based on the work proposed by Cooling et

al. [31], wherein a semi-empirical, iterating finite amplitude model is used to generate the phase information which acts as a reference. The model, assumes the hydrophone in the field to behave as a point receiver, and generates a linear phase response considering the characteristics of the source transducer. This method can be easily applied to the nonlinear, harmonic rich fields generated by HIFU sources, to aid in a complete complex deconvolution for the voltage to pressure conversion in the time domain. Fig. 2.1 shows our approach which is explained in detail in the coming sections.

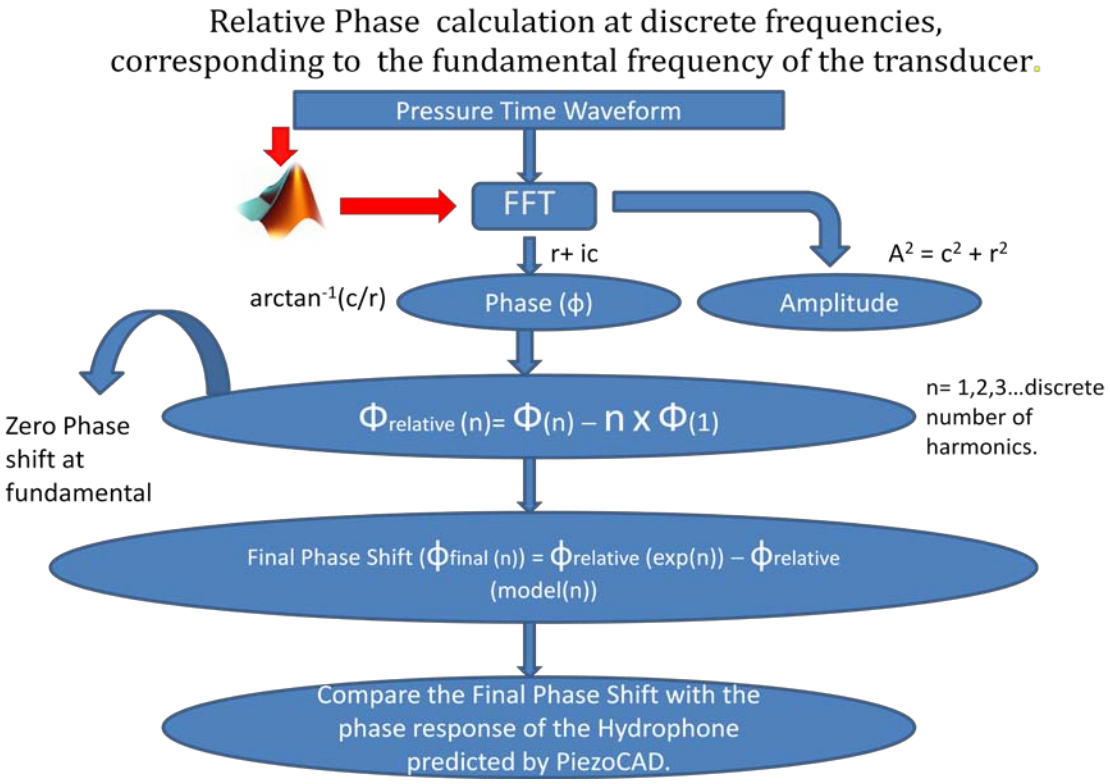

Figure (2.1) Flow diagram of the nonlinear approach to find phase characteristics

Acoustic field measurements in highly nonlinear fields are influenced by finite amplitude distortions generated by the media at high pressure amplitudes [32], with differences in the compressional and rarefractional pressure amplitude observed. Pressure variations

change the stiffness of the medium which, due to the dependence of the acoustic propagation velocity on the stiffness factor of the medium, generate a relative phasing between the harmonics. This in turn explains the differences in the rise and the fall time of the compressional and rarefractional pressure waveform [33, 34]. Hence it becomes critical for a complete understanding of acoustic wave pressure-time waveform in a broadband frequency range, to understand and correct the amplitude and the phase response of the field.

Any complex field can be represented by its amplitude and phase information. The amplitude is given by the square root of the sum of squares of the real and the imaginary parts and the phase can be calculated as arctan ratio of the complex components.

In the next section the hydrophones used in the phase measurements are described.

2.2 Hydrophone probes used in phase measurements

Hydrophones are electro-acoustic devices used to measure and characterize the field produced by an acoustic transducer in water. The hydrophone probe, depending on its amplitude sensitivity, generates the voltage time waveform corresponding to the pressure-time waveform generated in water at that particular position [2]. The probe should provide us with a linear relationship between the pressure in the field and the voltage observed. PVDF (PolyVinyliDene Fluoride) is the most frequently used polymeric piezoelectric material in hydrophone manufacturing. The popularity of PVDF is due to the fact that the acoustic impedance of water is relatively close to this polymer compared to other piezoelectric material, and hence at the surface there is maximum

transmission and minimum reflection. The thickness mode resonance of the hydrophone is governed by the thickness and the speed of sound within the active element and shifts towards higher frequencies as the active element becomes thinner, which in turn depends on half wavelength values for unrestricted membrane element, and quarter wavelengths for unidirectional needle type vibrations (Chapter 4 of [35]). Needle type and spot poled membrane hydrophones were used for various purposes in our study: to characterize the field generated by the source transducer, and to measure the pressure-time waveforms at the desired location, usually focal planes. Design details of these two types of hydrophones can be found in [36-40]. Very briefly, a membrane hydrophone uses a thin film 9-50μm thickness of PVDF stretched over a supporting ring. The membrane hydrophone shown in Fig. 2.2 is made up of two thin films glued together so that the outer two surfaces are at ground, and the inner surface contains the circular poled region. The active element, the small circular region at the centre typically of diameter 0.5-1mm, is both poled and electroded [38].

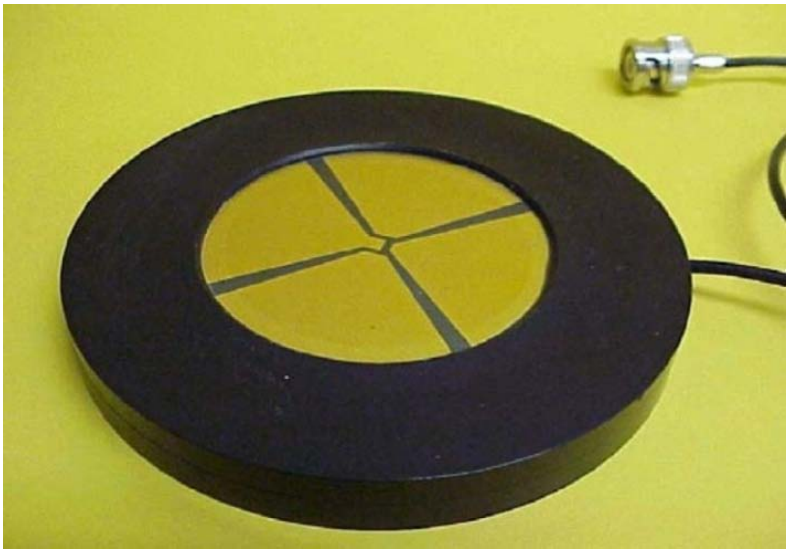

Figure (2.2) Bilaminar membrane hydrophone (Sonora Medical Systems, Longmont-Colorado, www.4sonora.com)

These membrane hydrophones, being free and loaded with water at both the ends, resonate at the fundamental thickness mode of half the wavelength (λ/2). In this study two hydrophones were used, the first one was a 500μm effective diameter, 50μm thick PVDF bilaminar Marconi membrane hydrophone terminated by 65 cm coaxial cable and placed in deionized and degassed water. The hydrophones were shielded with two outer gold electrodes electrically grounded, to minimize the Radio Frequency (RF) interference. The resonance frequency of this membrane hydrophone was 20 MHz. The second hydrophone used, was a 400μm effective diameter, 2*9μm thick PVDF bilaminar element Precision Acoustic membrane hydrophone; with a fundamental thickness mode resonance frequency of 70 MHz, and connected to a AH 2010 -100 preamplifier.

The Frequency response of a membrane hydrophone is relatively flat (~ 0.3 dB/MHz) below the resonance and decays at a rate of (~ 0.6 dB/MHz) beyond the resonance. Lum et al [28] designed and built a 4μm thick film membrane hydrophone from PVDF-TriFluoroEthylene copolymer, (PVDF-TrFE). This hydrophone had an extended bandwidth of 150 MHz and reliably determined the temporal and spatial characteristics of diagnostic transducers in the frequency range of 10-40 MHz.

For completeness, a needle hydrophone is briefly discussed.

Because of its physical size and, ease of use and alignment, in this study a needle hydrophone was used to capture the surface pressure and the apodization function.

However as discussed below, this hydrophone design is not well suited to be phase calibrated using the nonlinear approach.

The needle hydrophone, shown in Fig. 2.3 has a quarter wavelength resonating frequency (λ/4), and an active element diameter around 0.5 to 1mm.

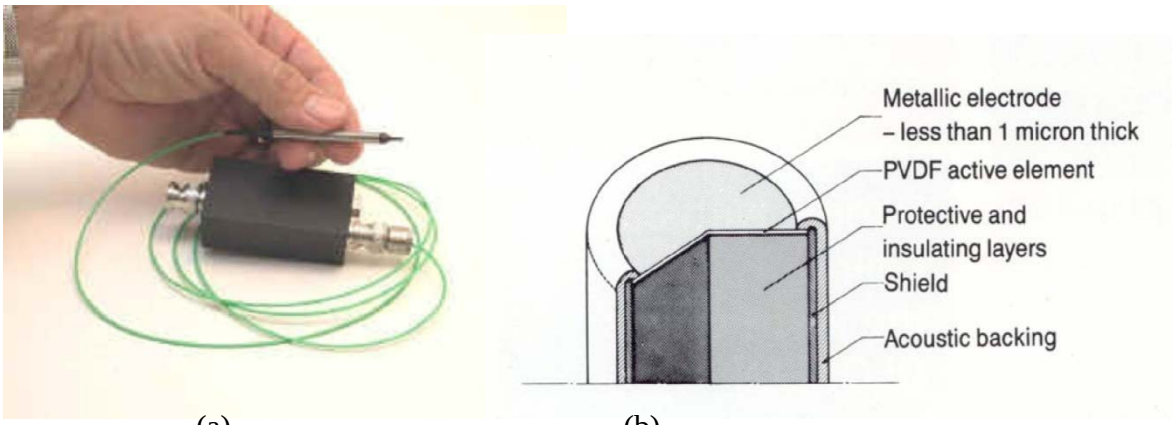

(a) (b)

Figure (2.3) (a) Photograph of a needle PVDF hydrophone and (b) the details of the sensor element. (Courtesy of Force Institute, Copenhagen-Denmark, www.force.dk)

The hydrophone used in the study did not use preamplifiers and a brief discussion below is needed to facilitate the results of the measurements presented in Sections 3 and 4.

Hydrophone converts the ultrasound pressure amplitude present in the field, to the corresponding voltage waveform on the oscilloscope, where the loaded oscilloscope or network analyzer system amplitude sensitivity is given by $M_L(f) = \frac{voltage}{pressure}$. In order to account for the electric load connected to the measurement system, measured or loaded system response is converted to end of the cable open circuit sensitivity of the hydrophone, which also helps to determine the open circuit sensitivity. The end of the cable loaded sensitivity, M_L , is determined by the Eq. (1), wherein M_c is the end-of-cable open-circuit sensitivity (Chapter 8 of [41]).

$$M_L = M_c \sqrt{\frac{\{\mathrm{Re}(Z_{el})\}^2 + \{\mathrm{Im}(Z_{el})\}^2}{\{\mathrm{Re}(Z_{el}) + \mathrm{Re}(Z)\}^2 + \{\mathrm{Im}(Z_{el}) + \mathrm{Im}(Z)\}^2}} \quad (1)$$

The real (Re) and imaginary (Im) Z_{el} are components of the complex impedance of the measuring oscilloscope, and the real and imaginary Z represents the complex impedance of the hydrophone respectively. Complex impedance components can be calculated, assuming the parallel circuit resistance R_L and parallel capacitance C_L as the load by Eqs. (2) and (3):

$$\mathrm{Re}(Z_{el}) = \frac{R_{el}}{1 + \omega^2 R_{el}^{\ 2} C_{el}^{\ 2}} \quad (2)$$

$$\mathrm{Im}(Z_{el}) = \frac{-\omega R_{el}^{\ 2} C_{el}}{1 + \omega^2 R_{el}^{\ 2} C_{el}^{\ 2}} \quad (3)$$

Here ω is the angular frequency $2\pi f$, and f is the frequency of $M_c(f)$. If the impedance of the load-hydrophone system is capacitive, the end of cable sensitivity reduces to Eq. (4).

$$M_L = M_c \frac{C_a}{C_a + C_c + C_s} \quad (4)$$

C_a, C_c, and C_s are hydrophone element, coaxial cable, and the stray capacitances respectively. As can be observed in Fig. 2.4, the major loading on capacitance C is due to the capacitance of the coaxial cable, C_c. This capacitance is proportional to the cable length and for coaxial cable used was determined to be about 100 pF/m. This value is

large compared to the piezoelectric element's capacitance, which is typically on the order of 0.3 to 3pF. Hence cable length is one of the major sources of capacitance which plays a major role in hydrophone sensitivity. Due to transmission line phenomenon, cable lengths also produce distortions in the pressure-time waveforms. These cable ringing distortions can be limited by minimizing the cable length, using a preamplifier to measure data, or using a low pass filter as discussed in [41, 42].

In the studies conducted for this dissertation, loading corrections were not required as the same oscilloscope was used for both, real field measurements and the calibration. In order to compare our results with previously published results [31], preamplifiers were not used in the study, hence hydrophones were connected directly to oscilloscope which loaded them with 1 MΩ terminations along with a 15 pF capacitance in parallel.

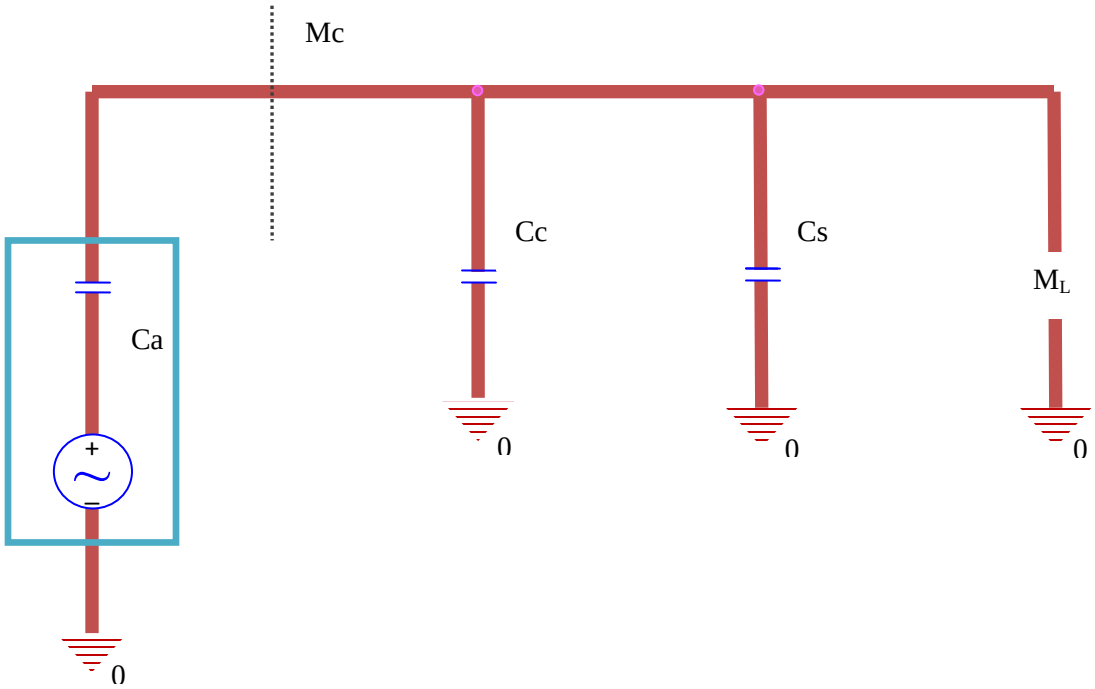

Figure (2.4): Schematic representation of the line capacitance effects on end-of-cable sensitivity. C_a, C_c, C_s are the hydrophone element, coaxial cable, and stray capacitances respectively. M_c and M_L are end of the cable loaded and end of cable sensitivities respectively. Chapter 8 of **[**41**]**

2.3 Nonlinear wave propagation and the JW model

The degree of nonlinearity depends on the medium through which the ultrasound wave propagates and the excitation level of the acoustic source. The velocity of the acoustic wave depends on the stiffness and the density of the medium, which alters when the pressure of the compressional peak of the wave exceeds a certain level. As the stiffness of the medium increases with the pressure, the compressional pressure peak amplitude starts propagating faster and leads the rarefractional wave. The rise time of the compressional peak decreases, the frequency bandwidth broadens and the content of harmonics increases leading to the distortion of the original sinusoidal waveform. These nonlinear distortions can also be appreciated by the different compressional and rarefractional pressures being observed at different nonlinearities. As the pressure amplitude generated by the source increases, these distortions also increase. Other factors which can enhance this distortion are: increasing distance from the source, increasing electronic focusing gain and higher frequencies, where the waveform finally obtains a saw tooth shape. The generated nonlinearity leads to an energy transfer from the fundamental to the higher harmonics, which can be up to an order of 40% [33, 34]. A detailed description of the nonlinear acoustics theory can be found in Chapter 16 of **[**35**].**

The degree of nonlinearity of the pressure wave generated in the medium by the source can be evaluated by taking into account the nonlinearity propagation parameter σ_m **,** which can be defined as Eq. (5) for a circular focused source [2, 43].

$$\sigma_m = \frac{\beta \omega z p_m}{\rho c^3} \frac{1}{\sqrt{G^2 - 1}} \ln\left(\sqrt{G^2 - 1} + \sqrt{G} \right) \qquad (5)$$

Where β is the coefficient of nonlinearity that is equal to 3.5 for pure water at 20 degrees Celsius, z is the distance from the transducer, ω is the angular frequency, $\omega = 2\pi f_c$, ρ is the water density and c is the velocity of sound in water, G is the linear focusing gain designated by $G = \frac{r_o}{z}$, r_o is the transition distance or Rayleigh length given by $r_o = \frac{\pi d^2}{4\lambda} = \frac{\omega d^2}{8c}$ (d is the diameter of the source and λ is the wavelength in water for fundamental frequency, f_c), p_m is the mean peak cycle acoustic pressure at the point in the acoustic field corresponding to the spatial peak temporal peak acoustic pressure at axial distance, z. There is little or no nonlinearity observed for values of $\sigma_m < 0.5$. The value of peak pressure amplitude at the fundamental differs from that calculated without any nonlinearity by less than 5%. For values of $0.5 < \sigma_m < 1.5$, the pressure amplitude measured in the half octave band centered at fundamental frequency is decreased from the one observed without any nonlinearity factor by 5% - 25%. For high nonlinear fields the values of σ_m are above 1.5, and there is considerable energy transfer to the higher harmonics generated in the field. The differences observed are over 25% as compared to the linear measurements [2].

In this work the nonlinear model was needed to obtain initial quantitative information about the pressure-time distortions and harmonics observed. To model this nonlinear field generated in a medium, Dr. Janusz Wójcik designed and coded a semi empirical and iterative simulation, known as JW model after his name [44]. This model was used here to predict the pressure-time response generated by circular spherically focused transducers. The model can also predict the field architecture produced by rectangular

mechanically and electronically focused transducers, at any point across the acoustic field in front of the source, taking into consideration all the medium losses and properties.

The JW model is based on the modified Khokhlov-Zabolotskaya-Kuznetsov (KZK) equation, representing the acoustic field generated in a nonlinear and lossy medium, and is given by the Eqs (6)-(10), [44]:

$$\Delta\Phi - \partial_{tt}\Phi - \partial_t A\Phi = q\partial_t\left(\partial_t\Phi\right)^2 + 2q_1 L\left[\Phi\right] \quad (6)$$

$$\mathrm{L}\left[\Phi\right] \equiv \frac{1}{2}\left[\left(\nabla\Phi\right)^2 - \left(\partial_t\Phi\right)^2\right] \quad (7)$$

$$q \equiv \frac{P_o\left(\gamma+1\right)}{2\rho_o c_o^2}, q_1 \equiv \frac{P_o}{\rho_o c_o^2} \quad (8)$$

$$\mathrm{A}\Phi = \mathrm{A}\left(\mathrm{x}\right)\overset{\otimes}{_{\mathrm{x}}}\Phi\left(\mathrm{x},\mathrm{t}\right) \quad (9)$$

$$A\left(x\right) = \left(\hat{F}\right)^{-1}\left[a\left(e \bullet K\right)\right] \quad (10)$$

Where $\Delta = \nabla\cdot\nabla$ is the Laplace operator, $\nabla\cdot$ is the divergence operation and ∇ is the gradient operator. Φ is the normalized acoustic potential, P_o is the characteristic absolute peak pressure value at the source surface, ρ_o is the equilibrium density, c_o is equilibrium sound velocity and *(x,t)* are the normalized space and time coordinates. $\gamma = c_p c_v$ is the exponent of the adiabate and c_p *and* c_v are the specific heats at constant pressure and volume, respectively. γ = B/A+1 where B/A is the nonlinear parameter [44]. Operator A can be described as in Eqs. (9), (10), where *A(x)* is the kernel of the convolution $_{x}\otimes$ with

respect to the space variable; *e* is the unit vector in the direction of the real component of the complex wave vector *K*.

Unlike other nonlinear acoustic field simulation models, the JW model, as a boundary condition, requires the apodization curve which gives a mathematic reproduction of the surface pressure amplitude profile of the acoustic source, and is generated by a 1D scan of the surface of the source along its diameter. This semi-empirically determined function gives a better representation of the surface of the transducer than an assumption for it to follow the Gaussian distribution, as used by other simulation models. The final solution generated, after all the parameters have been given as an input to the program, is in a form of complex Fourier spectra of the field generated by the source. The complex spectrum can further be used to extract phase and amplitude information for desired purposes.

For our experiments, only spherically focused sources were used to generate the acoustic field and hence, the boundary conditions of the excitation signal could be represented as a spectral component of the time domain function:

$$C_n(0,r) = C_{bn} e^{-\frac{ink_0 r^2}{2F_g}} \tag{11}$$

$$C_{bn} = 0 \quad \text{for} \quad r \geq a, k_0 = \frac{\omega_0}{c_0} \tag{12}$$

Furthermore, pressure pulse at the source surface is represented by Eq. (13), which is critical in determining the apodization function of the source.

$$f(t)=\left(1-\left|\frac{t-t_c}{t_s-t_c}\right|^m\right)\sin\left[\omega(t-t_c)\right] \qquad (13)$$

$$f(t)=0 \quad \text{for} \quad t\notin(t_s,t_e)$$

Here m = 2 and t_s, t_c, t_e are times of start, central part and of the end of the pulse, respectively. These conditions were suitable for the boundary pulse at the surface of the spherically focused source, assuming a parabolic lens located at the boundary. The plane wave front was generated from the transducer source and then transformed into a sector of the focused spherical wave with a focal length F_g.

Boundary conditions discussed in the previous parts of this dissertation, Eq. (6)-(13), were plugged into Silverfrost FTN95 [www.silverfrost.com]. This platform ran the FORTRAN codes on my personal Microsoft OS laptop computer, to simulate the nonlinear JW model using Eqs. (11)-(13). A MathCAD 14 program firstly is used to arrange the parameters required in the desired format for the FORTRAN program to calculate the complex spectra. Another MathCAD program was also used to graphically represent the results obtained. As discussed earlier, the JW model simulates both the linear and the nonlinear fields for the desired parameters. For the linear conditions, the numerical algorithm described by Eq. (14) is used. For this case, the number of spectral components was equal to the number of components used to describe the boundary conditions.

$$C_n(z+\Delta z,r)=B^{-1}\left[H(n,k_r,\Delta z)\cdot B\left[C_n(z,r)\right]\right] \qquad (14)$$

$$n = 1,2,3,\ldots N$$

Here *B*[.] is the Fourier-Bessel transform of the order 0, $C_n(z + \Delta z, r) = B[C_n(z,r)]$, $B^{-1}[.]$ is the inverse transform, k_r is the radial component of the wave vector. The Hankel transformation (*H*) of the Green function of the propagation equation is given by Eq. (15)

$$H(n, k_r, \Delta z) = e^{i\Delta z\left(\sqrt{k_n^2 + k_r^2 + 2ik_n a(n\omega_0)} - k_n\right)} \quad (15)$$

Function *H* propagates the wave field from the plane located at *z* to the next plane located at $z + \Delta z$ axial distance. The absorption coefficient is given by $a(n\omega_0) = \alpha_{l*}(\omega_0 / 2\pi)^l * n^l$; (n, *l*= 1, 2, 3, … N), where α_l and the value of *l* depend on the propagation medium. Nonlinear propagation conditions were simulated using Eqs. (16), (17)

$$C_n(z + \Delta z, r) = B^{-1}\left[H(n, k_r, \Delta z) \cdot B\left[C'_n(z, r)\right]\right] \quad (16)$$

$$C'_n(z, r) = NL^n\left(\{C_l(z, r)\}\right) \quad (17)$$

$$n, l = 1,2,3,\ldots N$$

NL is the nonlinear operator representing the interaction between the spectral component $\{C_n\}$ and the generating new components along the transmission path *z*. The details of *NL* were explained in [44, 45]. To minimize the computer calculation time, the number of spectral components were not equal to the number of components used to describe the boundary condition; but it depended upon the degree of the nonlinearity and the interaction between the nonlinear components. Also, the numerical method used here was

dynamically selectable from the second order Lagrange method to the fourth order Runge-Kutta method. The absorption coefficient used in Eqs. (16), (17) were assumed to be dependent on temperature, and the polynomial approximation described in [45] was used.

The pressure-time waveform was obtained by the Inverse FOURIER transform of the field spectrum.

The input normalized pressure-time waveform used as its Fourier series, and the apodization curve used as a representation of the source surface, is explained below.

2.4 Normalized pressure-time signal

Experimental linear and normalized pressure-time waveform was used as an input to the JW model, along with frequency, waveform envelope function's exponent coefficient ($E_{windows}$), number of cycles and repetition frequency. Eq. (18) defines the envelope function coefficient for the waveform used as the input to the model.

$$E_{windows}(x) = 1 - \left| \frac{2x}{np} - 1 \right|^{yy} \qquad (18)$$

Where x is the time index, np is the number of points in the waveform where the signal is nonzero and yy is the envelope's exponent coefficient.

To illustrate Fig 2.5 represents the waveform generated by MathCAD from Eq. (18) for a center frequency of 5 MHz, 10 cycles pulse and an envelope coefficient of 20. The y axis

is the normalized pressure amplitude and the x axis represents the retarded time normalized to 2π.

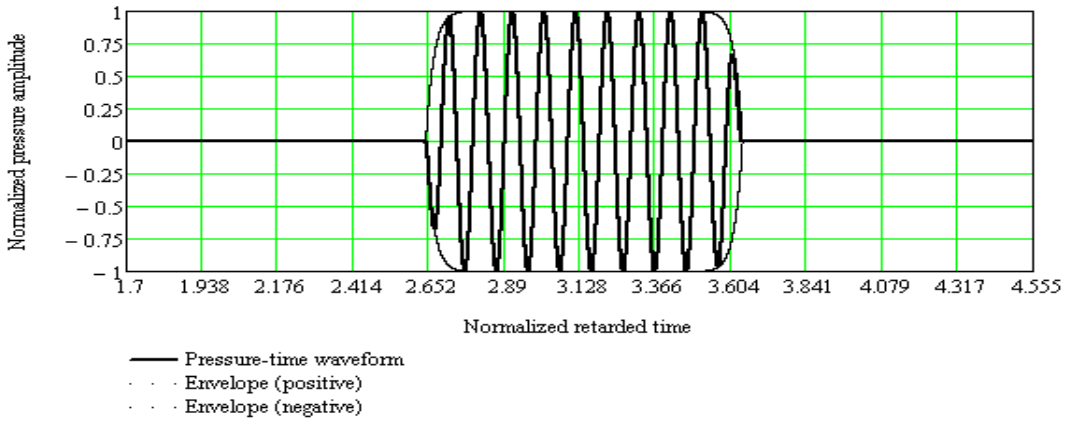

Figure (2.5): Normalized pressure-time waveform generated by JW nonlinear model, used as input for simulation of burst with of 10 cycles, 5 MHz center frequency, $E_{windows}$ of 20. The Y axis is the normalized acoustic pressure and the X axis is the retarded time normalized to 2π.

Fig 2.6 represents the frequency spectrum centered at 5 MHz, generated by JW simulation and used as one of the boundary conditions for the model.

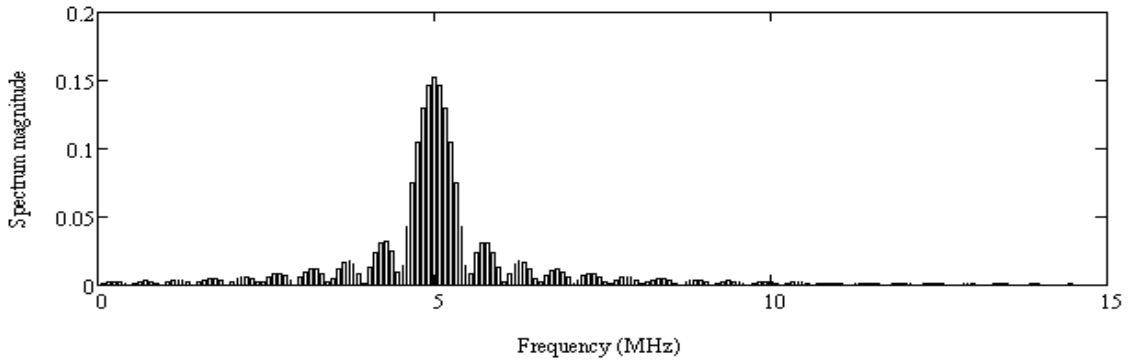

Figure (2.6): Spectrum pulse of the normalized pressure-time waveform modeled with the parameters of fundamental frequency: 5 MHz, 10 cycles and envelope coefficient of 20.

2.5 Surface apodization function

Surface apodization function acts as a boundary condition to represent the surface pressure profile of the source transducer. The FORTRAN program allows any function to be set as the apodization function in a predefined format. This function can be generated by a MathCAD program, where a 1D surface scan is given as an input along with the effective diameter of the transducer. As already noted the JW model can predict the acoustic pressure-time signal for both circular spherically focused transducer and rectangular focused sources [45]; but for all the experiments discussed in Section 3, only circular spherically focused transducers were used. The value of the apodization function was measured for individual conditions and is discussed in Chapter 3.

Chapter 3: Methodology

In this chapter, the experimental setup and the methodology to develop and optimize the phase calibration technique, for membrane hydrophones in a field generated by the HIFU sources, up to a frequency of 100 MHz is described. Complex hydrophone calibrations were performed for two membrane hydrophones using two different HIFU sources, One operating at third harmonic frequency of 5 MHz and the other operating at 10 MHz fundamental frequency. The experimental results were compared with the results obtained from the commercially available PiezoCAD simulation model (Sonic Concepts) [46].

This Chapter has been divided into three parts. The first part explains the experimental setup consisting of the source, the receiver and the instruments involved in the measurement of the nonlinear pressure-time signal. In the second part, a detailed description of the nonlinear acoustic model execution and input parameters required to run the simulations are given. Finally the third part describes the phase calibration technique.

3.1 Acoustic source pressure-time waveform measurements

In this section, we explain the step by step method to generate and record the pressure-time waveform for the phase calibration of the membrane hydrophone based on the nonlinear JW model. Figure 3.1 shows the setup used for the measurement of the pressure-time waveform in a nonlinear field.

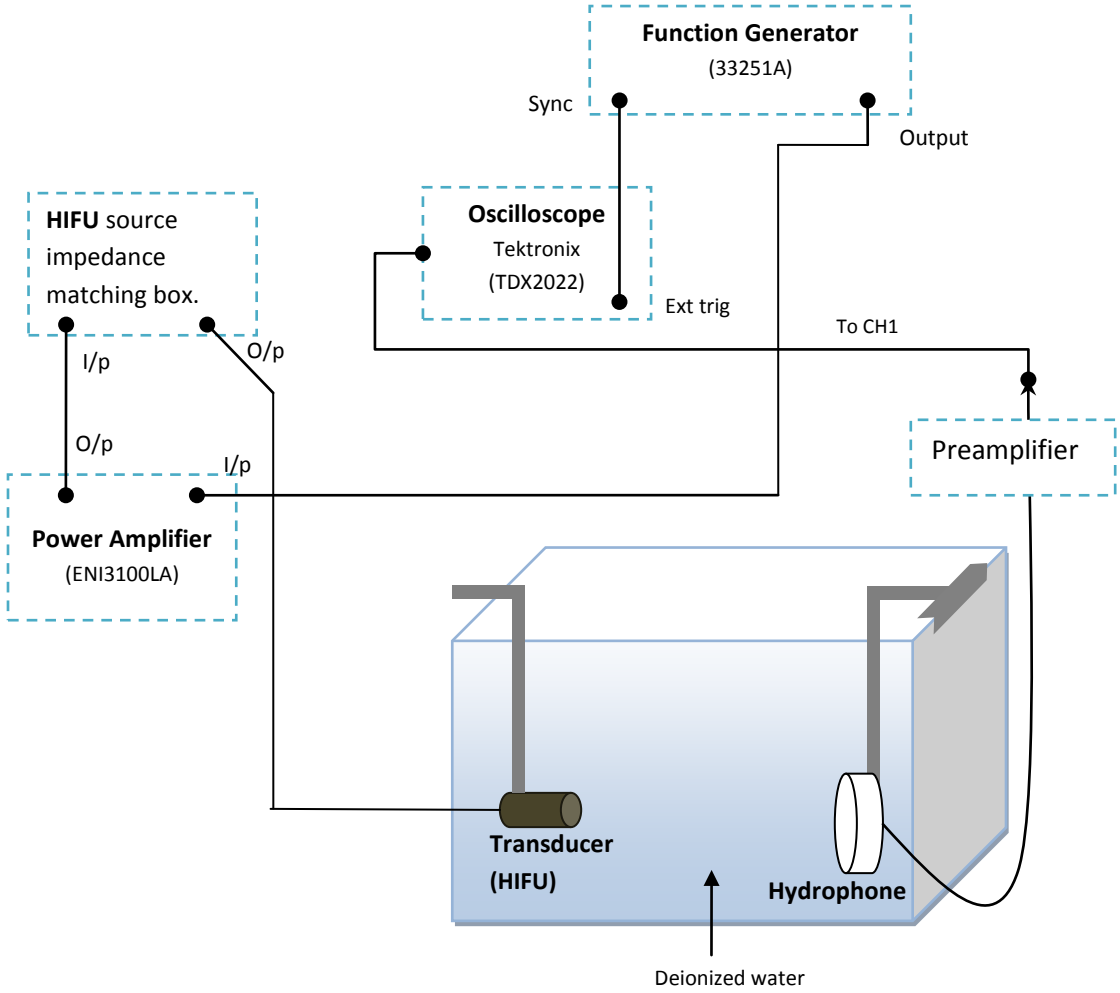

Figure (3.1): Experimental setup for acquisition of nonlinear pressure-time acoustic waveform using an acoustic source and a hydrophone in the focal plane.

All measurements were performed in a water tank of dimensions, 2m x 1m x 1m, using deionized and degassed water at a temperature of 22^{o}C. The Transducer-Hydrophone system was maneuvered by a XYZ manipulator, which was controlled by a program written in LabView 8. Focused HIFU source [46] of the desired frequency was mounted on specially designed holders and placed, horizontally under water. Membrane hydrophone was placed at the axial distance corresponding to the focal plane. Separate

holders to accommodate different shapes and the sizes of needle and membrane hydrophones were used. Special care was taken in making sure that no air bubbles were present at the surface of the source or the receiver. Air was blown by syringe to remove any residual bubbles present. An Agilent function generator (33251A) provided the input signal as a sine wave of the desired fundamental frequency, amplitude, delay and the number of cycles to a 55 dB Power Amplifier (ENI3100LA).

Signal from the amplifier of varying power level was fed directly to the oscilloscope using a 1:10 attenuator probe to test for any harmonics generated by the amplifier and verify that the harmonics generated only represent the nonlinear acoustic field. The output signal from the power amplifier was then applied to the HIFU source. The field generated by the source was sensed by the needle and membrane hydrophone at transducer surface and focal plane, respectively. To make sure that the hydrophone was aligned at the acoustic axis, measurements were taken at a point beyond the focus, realigned to maximize the signal and then moved back to the original focal point. No variation in the original voltage level at the oscilloscope verified the alignment. A voltage of 134 Vpp was applied to the 5 MHz transducer terminals from the power amplifier to generate 20 harmonics for measurements to cover 100 MHz frequency range. At the receiver end a 20 dB preamplifier, SEA 377, ONDA Corp., was used to amplify the output, and help align the hydrophone in a highly focused field at high frequencies. Phase response of the preamplifier was recorded and is provided in Fig. 3.2. Until 30 MHz the preamplifier had a flat phase response which then increased linearly with increase in frequency.

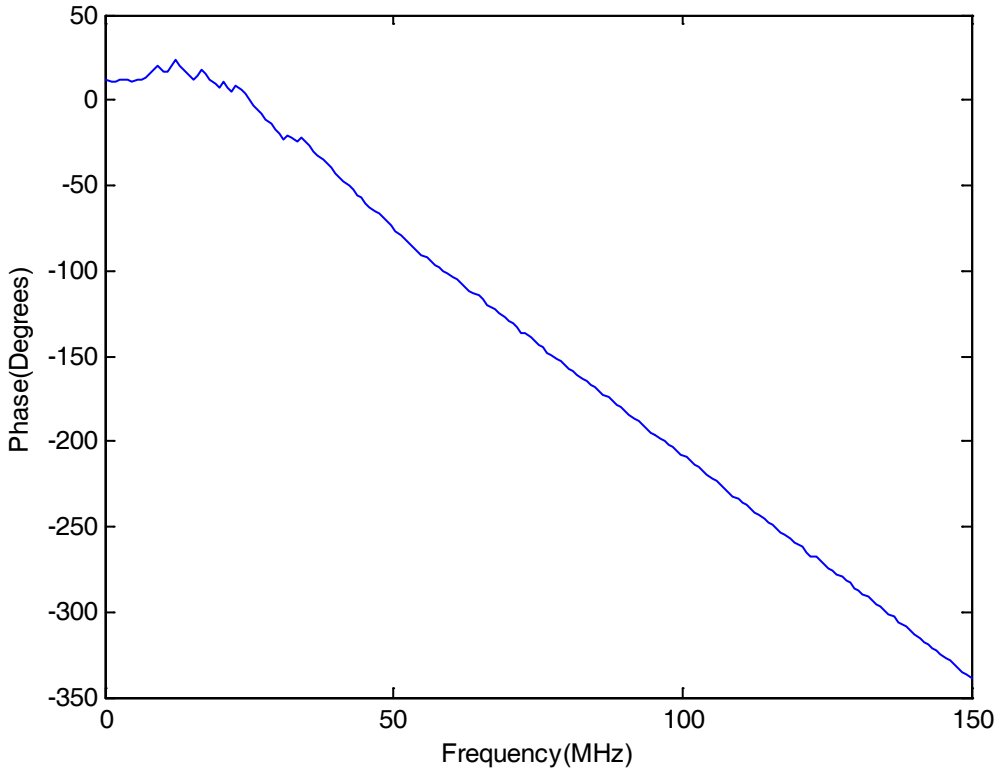

Figure (3.2): Phase response of the Preamplifier SEA 377.

It should be stressed that a preamplifier was not used during phase calibration, as its presence added a linear phase to the measurements and also limited the bandwidth due to clipping of the waveform observed at higher pressure levels above 4 MPa. A 50 Ω coupling was used for hydrophones with a 50 Ω matching preamplifier. When the measurements were done without the preamplifier, the hydrophones were connected directly to the 1 MΩ termination of the oscilloscope. The oscilloscope was connected to a PC, through a GPIB port and the signal was captured by the commercially available AIMS software (Onda, Sunnyvale). Both time and frequency domain information were recorded using this software. The pressure-time signal was then processed to obtain the amplitude and phase information, by a routine written in Matlab.

3.2 Acoustic source characterization

This section explains the steps taken to characterize the HIFU transducer to determine boundary conditions necessary to simulate the nonlinear field generated.

The first step undertaken to characterize the field produced by a HIFU source was to measure the pressure generated at the surface of the HIFU transducer. To one end as in Fig 3.1, a needle hydrophone was placed at a distance of 3 mm from the source on the acoustic axis and the voltage time waveform was captured. Next, using the amplitude sensitivity conversion factor for the hydrophone, the surface pressure amplitude was calculated. This close axial distance was chosen in order to only measure the direct wave without the interference due to the edge waves. It also ensures that the HIFU transducer was operating in a linear way and did not generate any harmonics. The transducer was scanned along the axis to locate the focal distance. A 2-D scan at the focal region of the transducer is shown in Figs 3.4 and 3.5, which displays the energy distribution of the field generated by the transducer at the focal plane. It also verifies that, as we go to higher frequencies, the focal area decreases. Another important parameter is the apodization function of the HIFU source used. A radial scan at a distance of 10mm from the surface of the source by a needle hydrophone was recorded, and fitted to a curve to obtain the desired equation for the function. The apodization function (see Eq. (19)) was input to the JW model as shown in Fig 3.9. For our experiments we have used a 1.52 MHz source, for its 3^{rd} harmonic frequency, and Fig. 3.3 shows the apodization curve being used for the calibration using a 5 MHz source. The function is the best fit for the curve in Fig. 3.3 and an analytical expression was derived which is given by Eq. (19).

$$A = 1 - \left(\frac{xx}{r}\right)^{px} - \left[fc\left[\cos\left(fxx \frac{xx}{r}\right)^2\right]^2 - fcf \,.\, fc\right] \bullet \left[\left(\frac{xx}{r}\right)^{pxb} - \left(\frac{xx}{r}\right)^{pxa}\right] \quad (19$$

Where ***xx/r*** is the normalized source radius and the parameters ***px, fc, fxx, fcf, pxa*** and ***pxb*** were: 1.9, 100, 1, 5, 2.0 and 2.001, respectively. These values were obtained by fitting the above equation to a curve by a routine written in MathCAD.

Fig 3.4 gives the contour representation of the 2-D scan of the focal region.

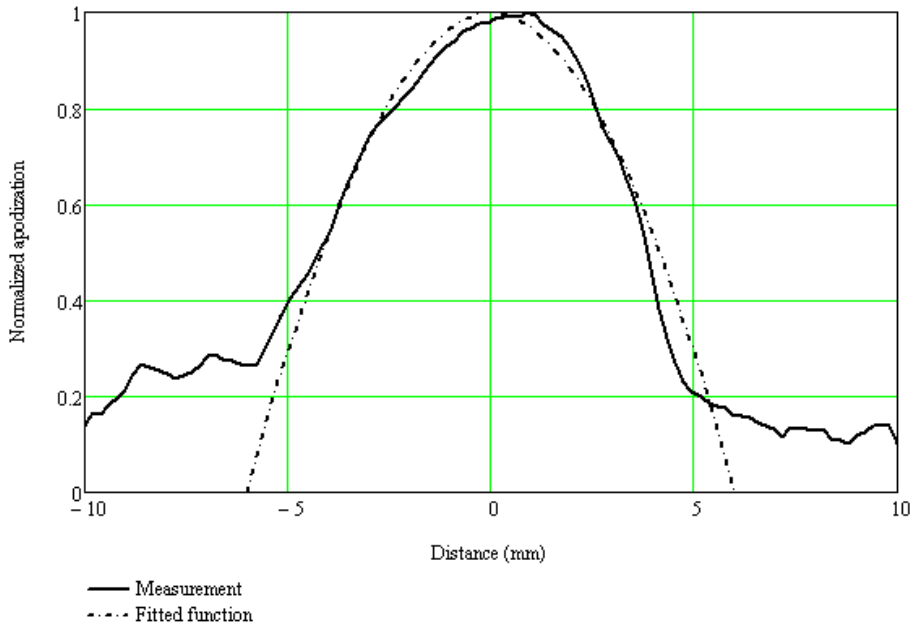

Figure (3.3): Comparison between the calculated normalized apodization function and the one obtained through the measurements performed at 10 mm axial distance from the surface of the 5MHz acoustic transducer.

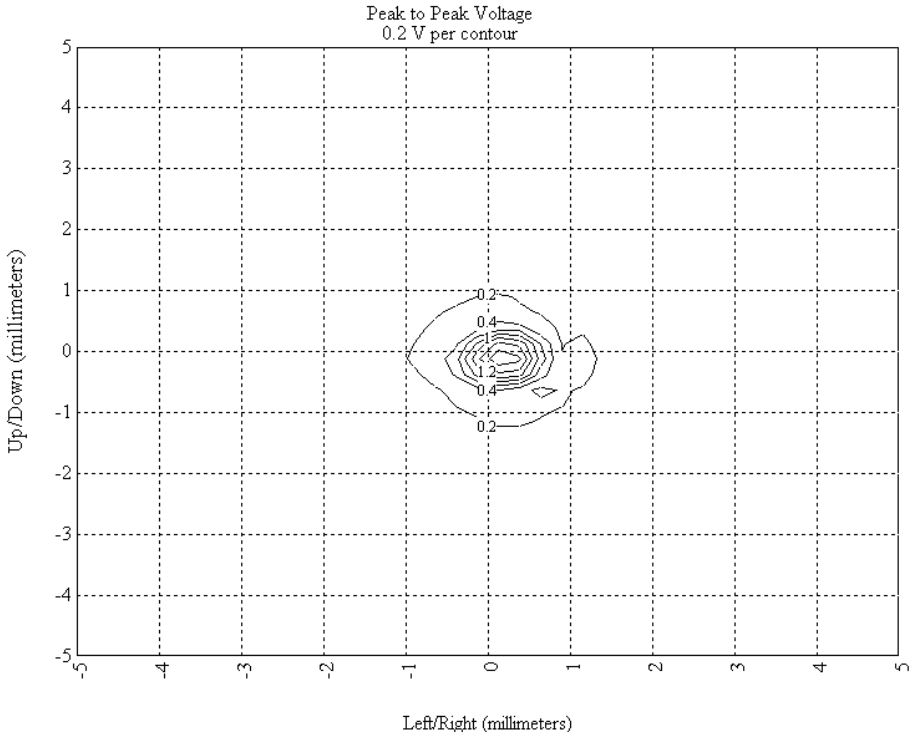

Figure (3.4): Contour plot of the isobars generated by 5 MHz HIFU transducer. The plot was obtained using needle hydrophone at the focal plane (35 mm axial distance from the transducer's surface).

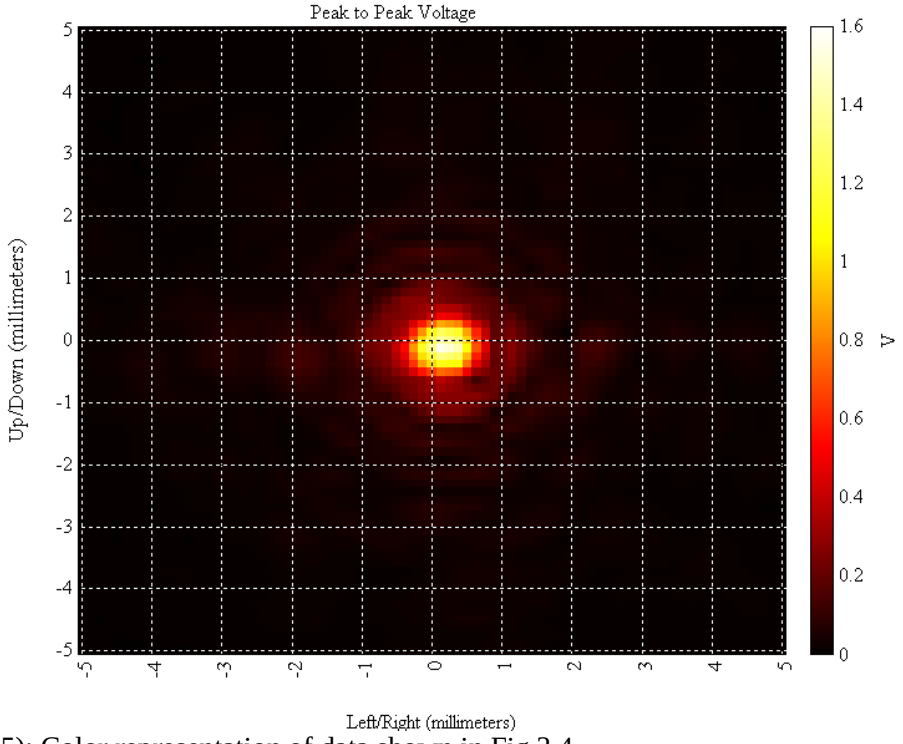

Figure (3.5): Color representation of data shown in Fig 3.4

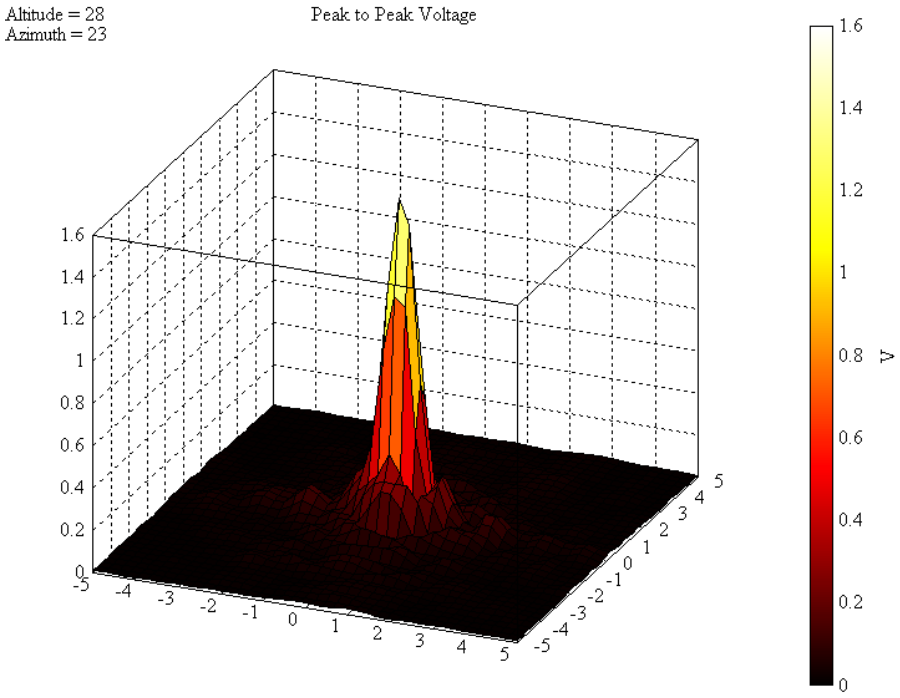

Figure 3.6: 3-D reconstruction of the isobar in Fig 3.5

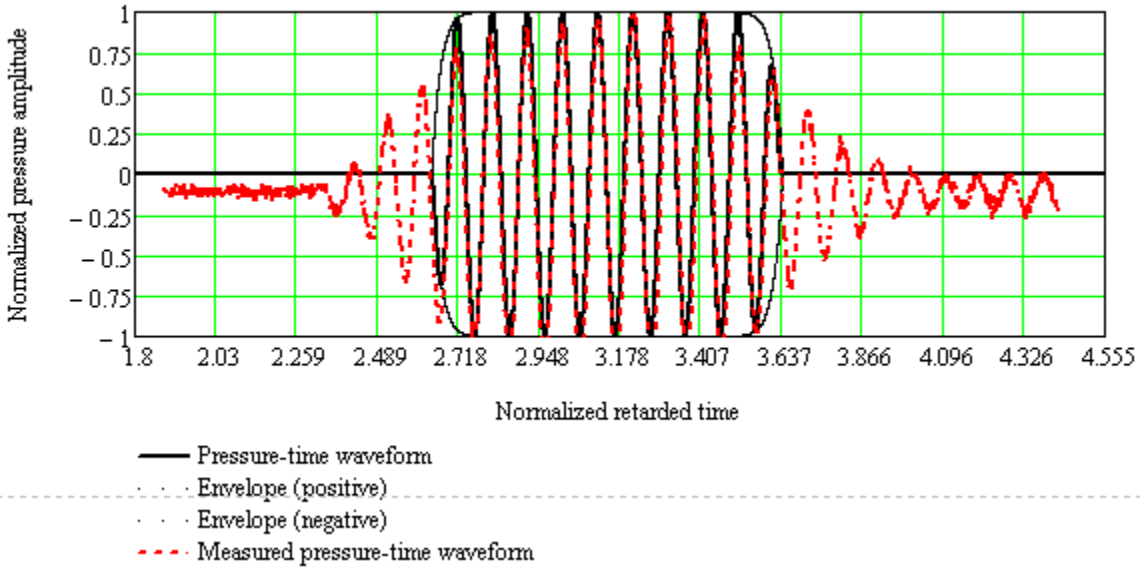

Figure (3.7): Comparison between the normalized experimental and simulated pressure-time waveform. The measurement was performed near the surface (3 mm) of the 5 MHz focal number HIFU acoustic source by the needle hydrophone.

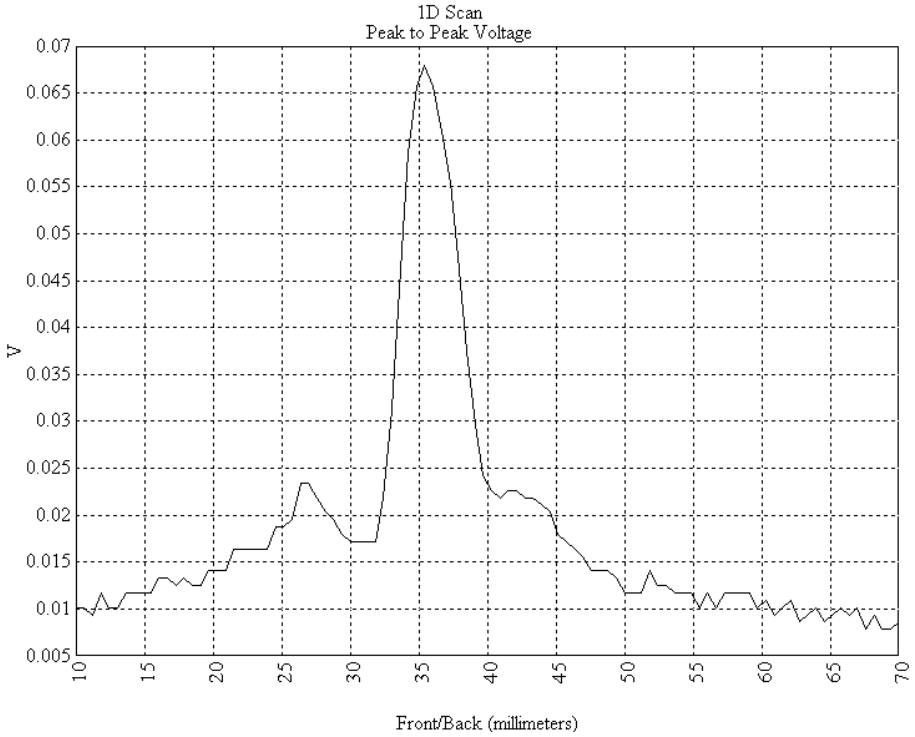

Figure (3.8) 1-D scan along the acoustic axis at low pressure amplitude corresponding to 0.013 MPa, to find the focal distance of the 1.52 MHz HIFU source used in the study by a needle hydrophone.

Figure 3.6 is the 3-D representation of the colored intensity of the contour plot in Fig 3.5. The tone burst waveform generated by the model for the 5 MHz HIFU source, 10 cycle waveform of envelope coefficient 20 at the surface was experimentally verified by a measured signal at the surface of the source by a 500μm needle hydrophone (NTR-07050589, and Force Institute – MI-583), and the comparison of the normalized waveform is given in the Fig 3.7. The focal distance was estimated by a scan along the acoustic axis of the transducer with a step size of 0.5mm and is identified in Fig 3.8 as 35.5 mm.

For the measurements at the surface of the source, membrane hydrophones were not used in order to minimize the reflections due to the design.

All the above transducer characterization experiments were done in a different water tank

of dimensions 75cm x 40cm x 45cm, containing degassed and deionized water. A XYZ micromanipulator with the minimum resolution of 10 microns was used to scan the surface and the acoustic axis. All scans were automatically performed by the stage controlled by commercially available AIMS software connected to the oscilloscope through a GPIB port to record the signal.

3.3 Nonlinear Field Simulation

Once the initial HIFU characterization data was acquired, the nonlinear simulation was performed according to the procedure shown in Fig 3.9.

The nonlinear JW model [44, 45] is coded in MathCAD and FORTRAN. In total there are three programs which consist of two MathCAD codes and one FORTRAN code. The first MathCAD program governs the rest of the simulation by storing the input boundary conditions in the format, which the FORTRAN compiler can understand. All the files created in MathCAD were stored in data file format. The input parameters which were required to be in the desired format for the 1st MathCAD include: Dimension of the source head (DimHE), Speed of sound (co), Carrier frequency (fcar), Number of cycles (LC), Experimental pressure-time waveform data file at the surface (ttt.prn), Power of the envelope (yy), Phase factor, Focal length (foc), Pressure at the surface of the source (Po), Density of the medium and Degree of nonlinearity (Mpp). Bondarytime.mcd also generated the normalized pressure-time waveform which was compared with our linear experimental waveform obtained at the surface. Transducer surface pressure-time data files in .PRN format, generated by BOUNDARYtime.mcd, were read by the FORTRAN program to simulate the field elements. The computational time varied with the frequency

and the pressure level at the surface of the source. As pressure generated by the source increased, the degree of nonlinearity generated in the water increased, leading to a higher

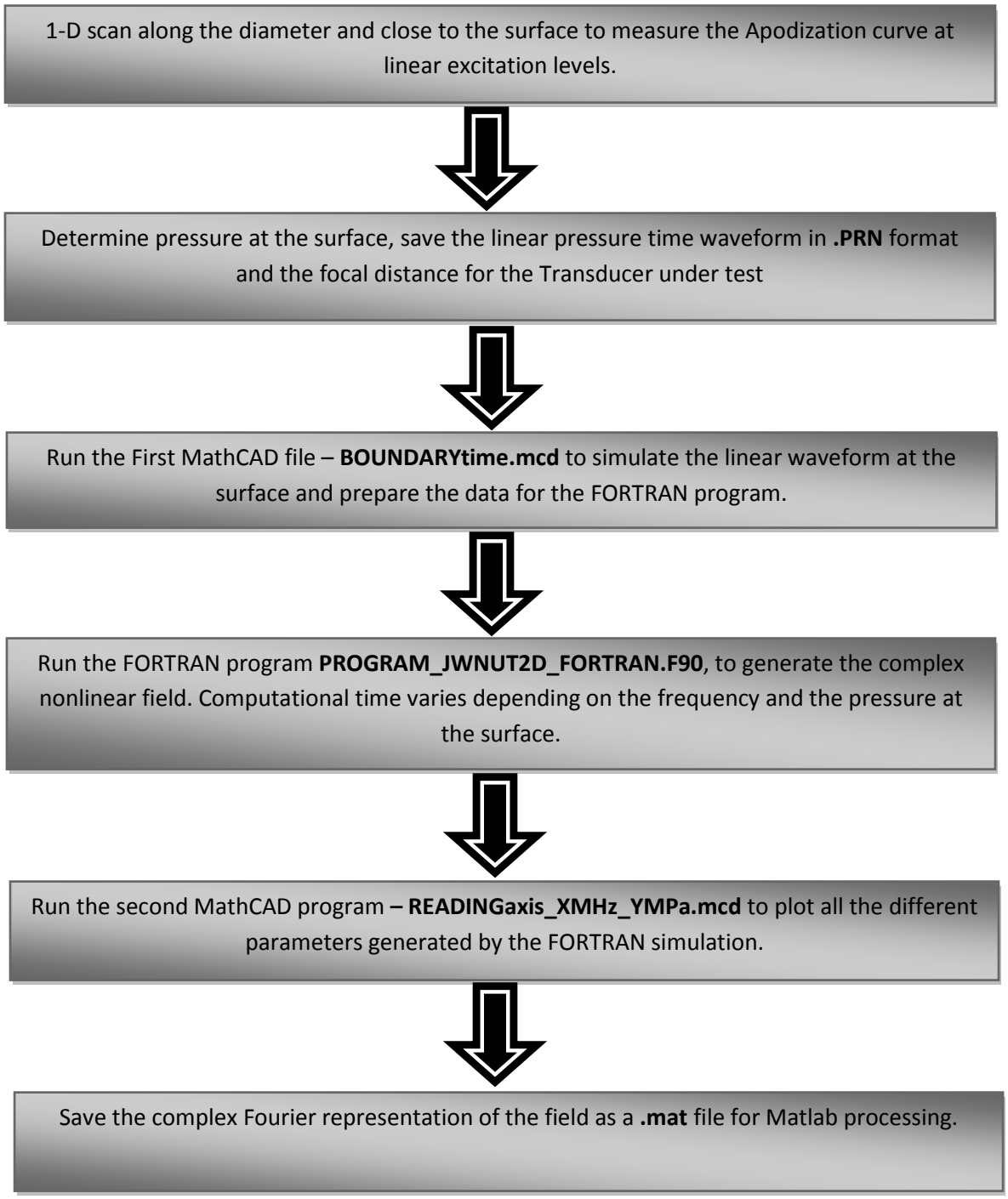

Figure (3.9) Flow diagram of the steps involved to run the JW simulation.

number of harmonics and hence, an increase in the computational time of the simulation. The maximum simulation time was observed at the focal plane, where the maximum number of harmonics was generated. Once the acoustic field was simulated by PROGRAM_JWNUT2D_FORTRAN.F90, the 2nd MathCAD program plotted the graphs required for observation. The 2nd MathCAD program also generated a Matlab data file (.MAT) which contained the complex field components, which were subsequently used to extract the amplitude and phase data by Matlab. Moreover the 2nd MathCAD also plotted the field distributions along the radius and the z axis.

3.4 Evaluation of the phase response

The phase response obtained from the nonlinear simulation calculations (JW model) and the experimental values were compared to obtain the phase shift for the membrane hydrophones. The unwrapped phase value obtained from the FFT'ed spectra corresponding to the harmonics generated by the model and those obtained experimentally by recording the signals obtained at the terminals of the membrane hydrophones were expressed with respect to the phase value determined at the fundamental frequency. This was done by introducing a phase shift to each harmonic phase value to obtain the phase at the fundamental as zero. Assuming the value of the phase of the experimental spectrum at the specific frequency to be $\boldsymbol{\varphi_{exp(n)}}$ where n is the number of harmonics and n=1 represents the fundamental frequency, which in this case was 5 MHz and 10 MHz for the two cases studied. The value of the relative phase with respect to the fundamental is given by Eq. (20), [31]:

$$\phi_{exp(n)} = \varphi_{exp(n)} - n^* \varphi_{exp(1)} \quad (20)$$

Similarly the model simulated phase at the frequencies specified by the harmonics is given by $\varphi_{model(n)}$. The value of the phase with respect to the fundamental frequency is given by Eq. (21).

$$\phi_{model(n)} = \varphi_{model(n)} - n^* \varphi_{model(1)} \quad (21)$$

Once the phase with respect to the fundamental was extracted, the total phase shift between the model and the experimental values was calculated according to Eq. (22). This shift represented the differences between the phases simulated by the model, assuming the hydrophone to behave as a point receiver in the field generated by a tone burst excited HIFU source.

$$\phi_{shift(n)} = \phi_{exp(n)} - \phi_{model(n)} \quad (22)$$

3.5 Hydrophone Simulation PiezoCAD software

In order to compare the final phase response calculated by using Eq. (22) with a reference for our test membrane hydrophones PiezoCAD, a commercially available software developed by Sonic Concepts WA, was used to simulate the phase response. This simulation package is used extensively to design and analyze the amplitude and phase response of a transducer or hydrophone. Desired central frequency, cable length, piezoelectric material, membrane thickness and shape, acoustic property of the loading medium, attenuation of the loading medium, are the input parameters required to simulate

the amplitude and the phase characteristics of the acoustic field sensed by the hydrophone under test. To simulate the membrane receiver, mechanical and dielectric losses have also been included in the model. Because of the transmission line model, the effects of coaxial cable resonances can be accounted for, as observed in the experimental data.

In the next section the results of the phase calibrations are presented.

Chapter: 4 Results

This chapter presents the experimental and theoretical results obtained after executing operations explained in Chapter 3 above. Firstly, the results obtained by the acoustic measurements using the nonlinear field generated by the 5 MHz and 10 MHz sources are presented. The results generated by the nonlinear JW model are then discussed, along with key parameters required to generate the complex field by simulation. Finally the phase calibration results are presented.

As discussed earlier, two membrane hydrophones were used in the phase measurement studies. Firstly, a 500μm diameter bilayered membrane hydrophone manufactured by GEC-Marconi Research Center, Chelmsford, UK, was calibrated according to the procedure shown in Fig 2.1. This hydrophone was hard wired with a 65 cm cable. This cable length was appropriate to verify the phase calibration technique. Another 400μm diameter membrane hydrophone by Precision Acoustics, Dorset, UK; was characterized according to the protocol discussed earlier. The Precision Acoustics hydrophone; which was custom made for operations it the frequency range up to 100 MHz and above, was connected to an adjacent preamplifier – AH2010-100, and it was used to observe the effect of a preamplifier on our phase studies.

Fig 4.1 represents the pressure-time waveform generated at the surface (3mm axial distance) of the HIFU source operating at third harmonic frequency of 5 MHz and excited by 134 V_{pp}.

Fig 4.2 gives the amplitude response of the FFT of the waveform, which clearly shows the degree of nonlinearity observed is minimal and the level of the first harmonic is lower than the fundamental by at least 30 dB.

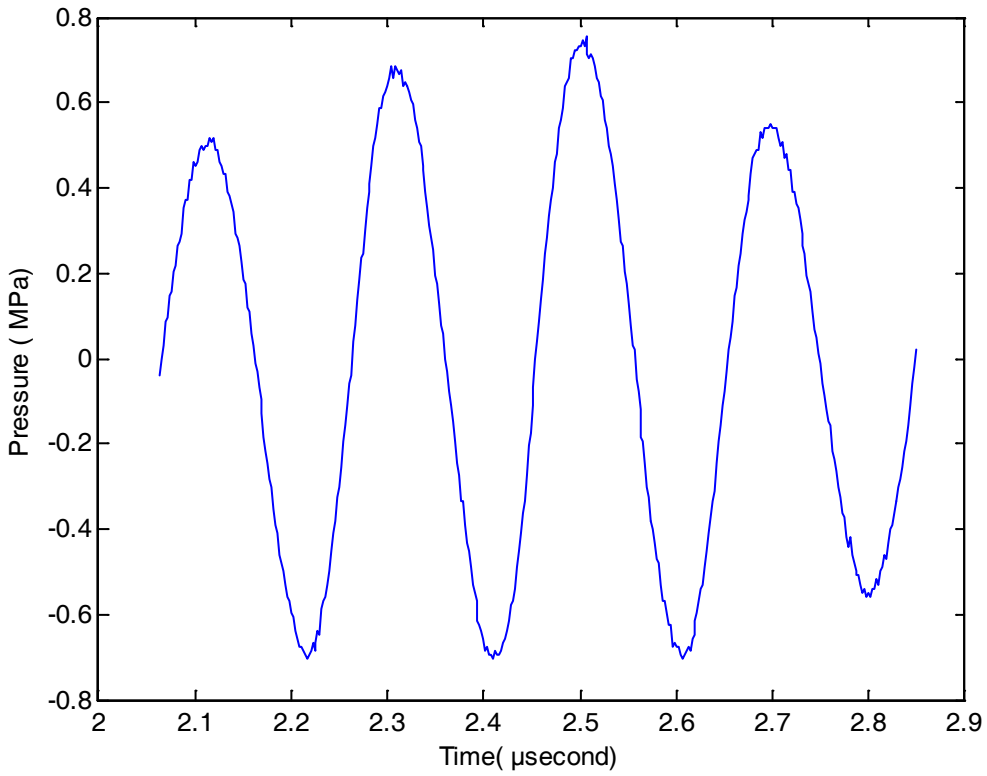

Figure (4.1) Pressure-time waveform recorded by the needle hydrophone (see Chapter 3) at the surface of the HIFU source operating at 5 MHz, 134 V_{pp}, and 4 cycles tone burst.

The axial pressure profile generated for different harmonics at 134 Vpp excitation are given in Fig 4.3.

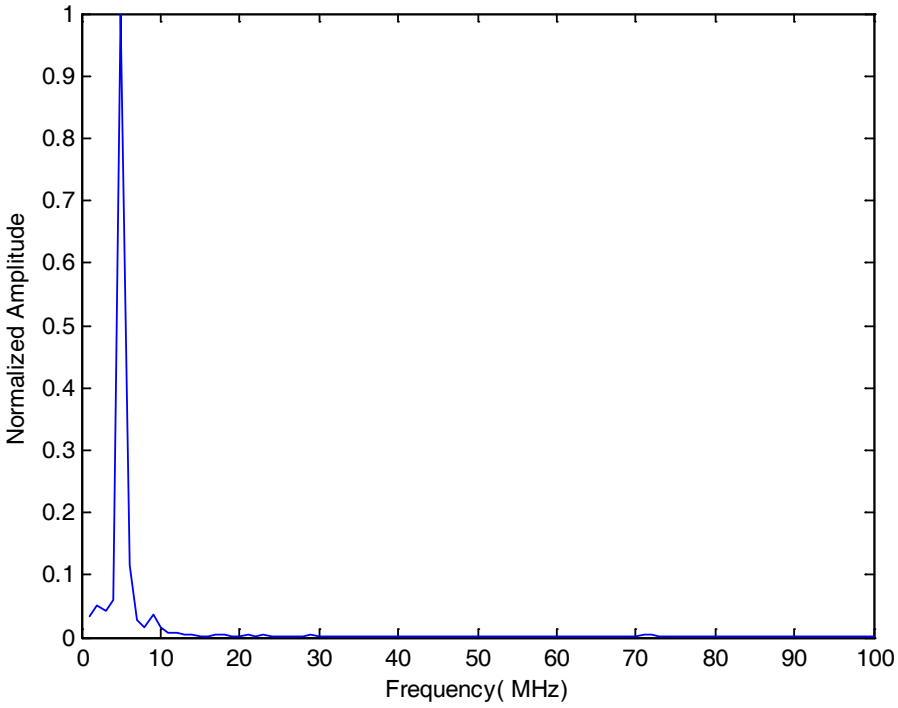

Figure (4.2) FFT of the pressure-time waveform recorded at the surface of 1.52 MHz HIFU source operating at its 3rd harmonic of 5 MHz. It confirms absence of harmonics at the maximum excitation voltage applied to the terminals of the HIFU source.

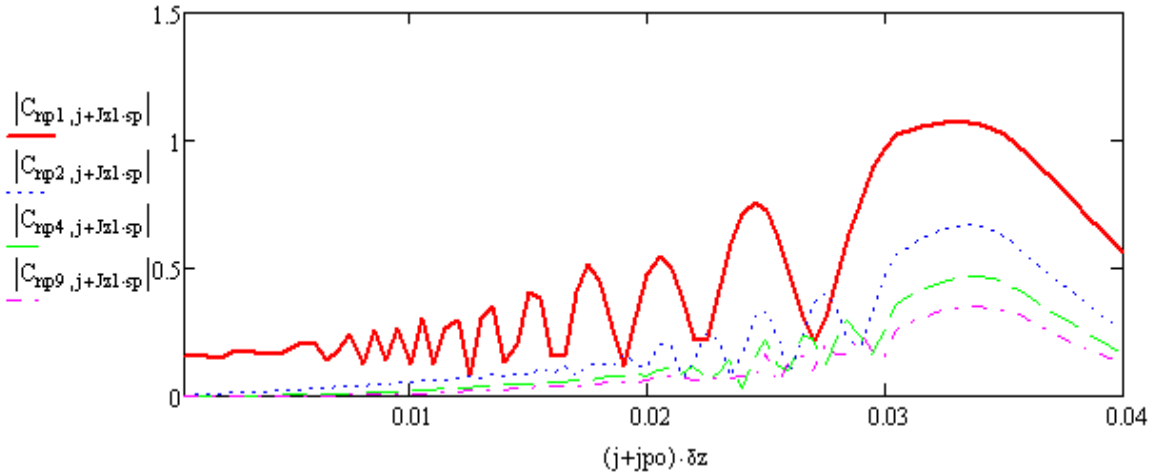

Figure (4.3) Pressure distribution along the acoustic axis, as estimated by the nonlinear JW model for 1.52 HIFU (at 3rd harmonic) source excited by 10 cycles at 134 Vpp: Fundamental (5MHz) (Solid red line), Second harmonic (blue dotted lines), Third harmonic (green dashed line), Fourth harmonic (dashed dotted pink lines)

The amplitude calibration of a very similar 50µm thick Marconi bilaminar membrane hydrophone and effective diameter of 500µm with the same cable length of 65 cm was described in [47]. The membrane hydrophone was calibrated until 100 MHz using a similar nonlinear technique. The fundamental resonance due to the thickness of PVDF used in the membrane hydrophone was 20 MHz and the resonance at 80 MHz was ascribed to the 65 cm cable attached to the hydrophone. These values of the resonating frequencies of the membrane hydrophone corresponded with the values discussed by [31] for their hydrophones with similar active element and cable length. Fig 4.5 presents the nonlinear pressure-time waveform recorded by the membrane hydrophone under test, with the HIFU source driven by an excitation voltage of 134 V_{pp}.

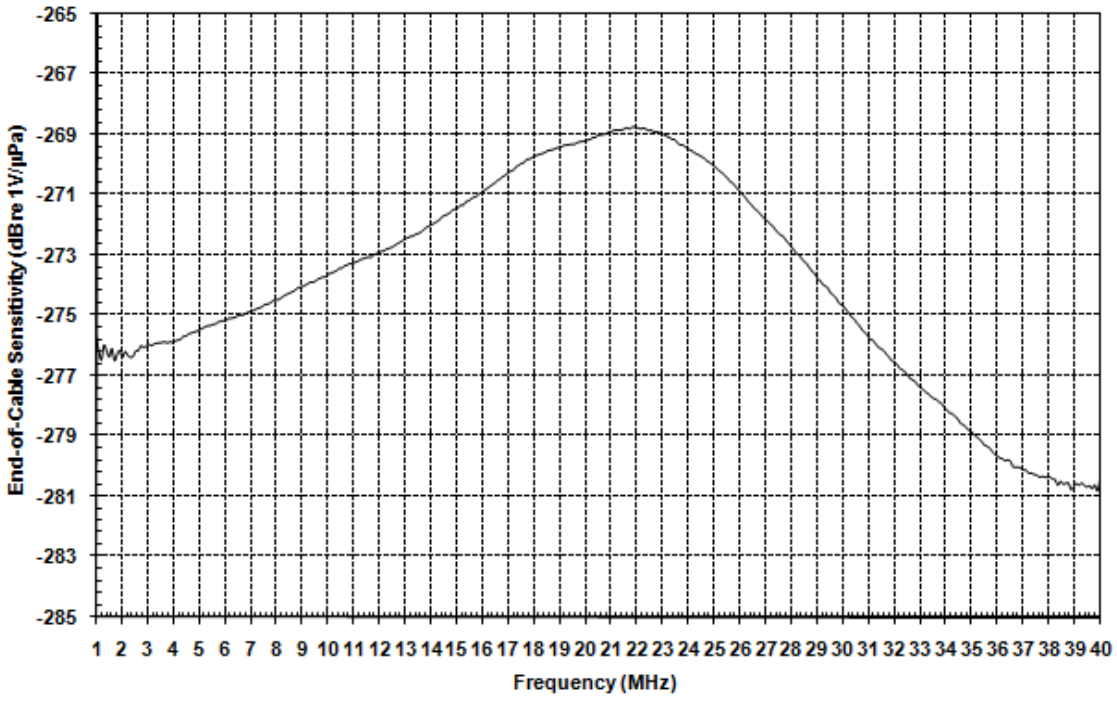

Figure 4.4 Amplitude sensitivity obtained by TDS method, of the Marconi hydrophone used in our study up to 40 MHz.

Prior to the phase measurements this hydrophone was (Amplitude) calibrated by Dr. Peter A. Lewin, and its frequency response is shown in Fig 4.4.

As shown in Fig 4.4 the amplitude sensitivity of this membrane hydrophone at 5 MHz was -275 dB re 1V/μPa and using this sensitivity value the pressure amplitude of the HIFU source was determined to be 6 MPa. The 134 Vpp value of excitation voltage generated a pressure of around 6 MPa at the focal plane. As shown in the following description 20 harmonics were generated by this level of excitation which enabled measurements in the frequency range of 5-100 MHz. Pressure time waveform generated by JW model by calculating the IFFT (Inverse Fast Fourier Transform) of the complex field generated is shown in Fig 4.6

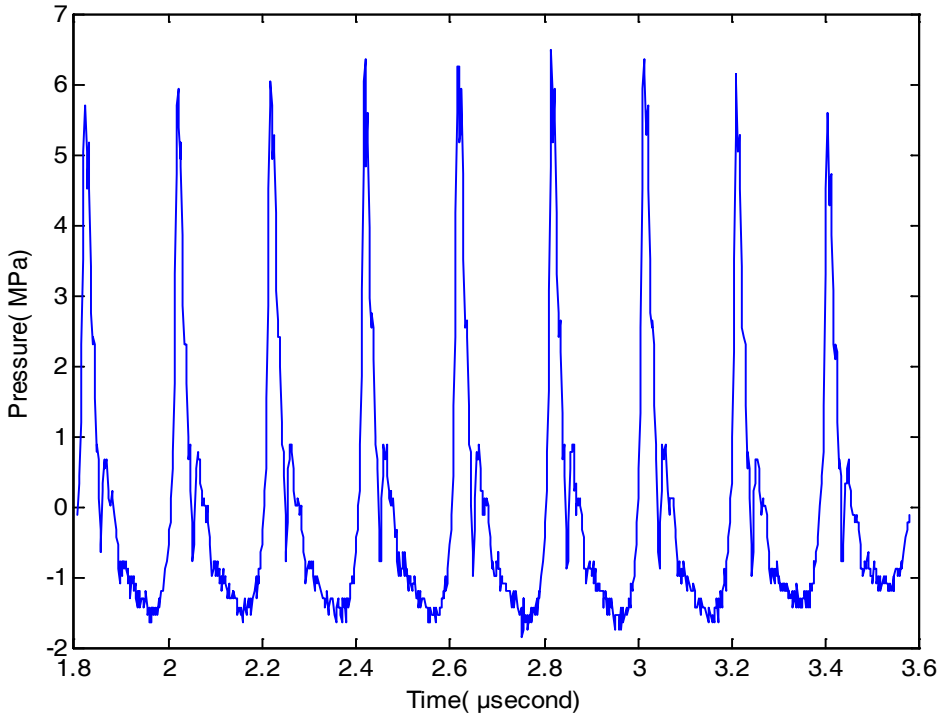

Figure (4.5) Nonlinear pressure-time waveform as measured by the Marconi Membrane Hydrophone and generated by the 1.52 MHz HIFU operating at its third harmonic of 5 MHz with excitation voltage of 134 V_{pp}.

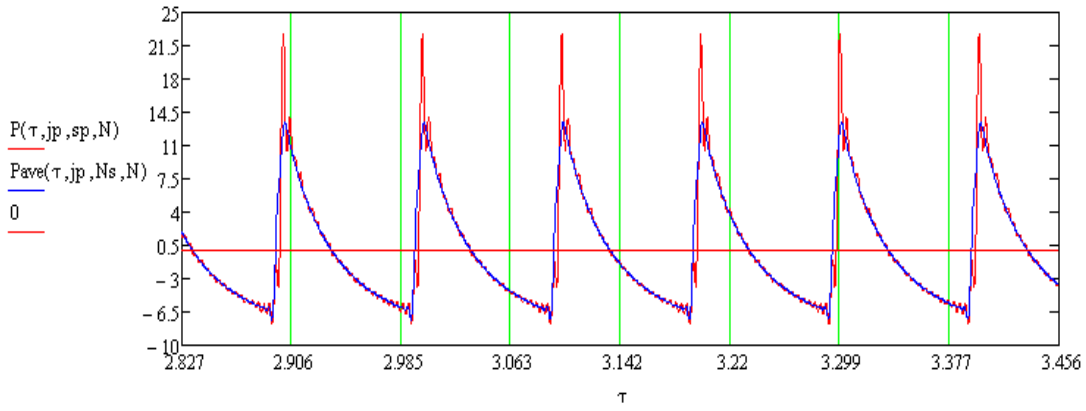

Figure (4.6) Scaled nonlinear pressure-time waveform as simulated by the JW model, corresponding to the input parameters: Surface Pressure 1.5 MPa and frequency of 5 MHz.

Figure 4.7 shows the normalized magnitude response of the pressure-time waveform shown in Fig. 4.5, obtained by applying a standard FFT algorithm on Matlab. Figure 4.8 compares the normalized amplitude response generated by the model and the experimental data shown in Figs 4.5 and 4.6.

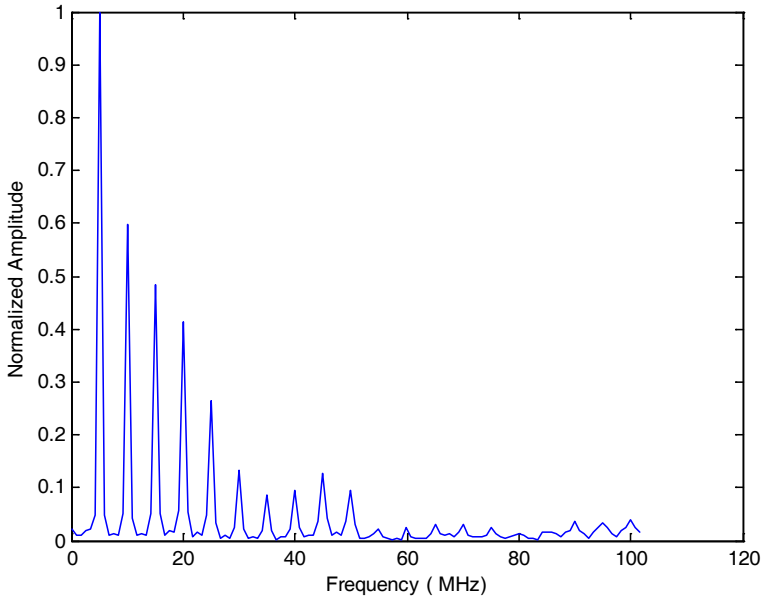

Figure (4.7) Amplitude of the FFT response of the experimentally measured pressure-time waveform of Fig. 4.5

The agreement between the JW model and the experimental data was verified by analyzing the pressure-time waveforms measured and JW model generated and comparing the number of harmonics. The model predicted generation of 20 harmonics, which were subsequently, measured using the Marconi hydrophone. In order to compare the phases determined by the model and those measured experimentally, both curves were shifted with respect to the fundamental frequency and are shown in Figs 4.9 and 4.10, respectively.

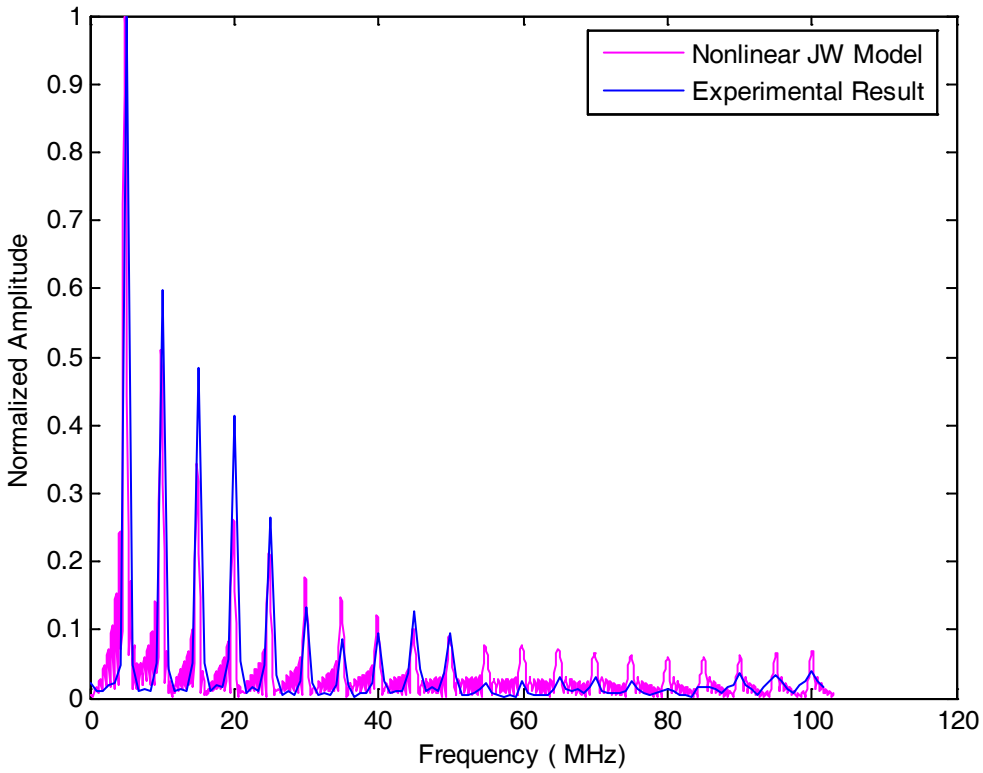

Figure (4.8) Amplitude of the FFT response of the experimentally measured pressure-time waveform Fig.4.5, (blue solid lines), and the amplitude response of the complex field generated by the JW model (magenta solid lines)

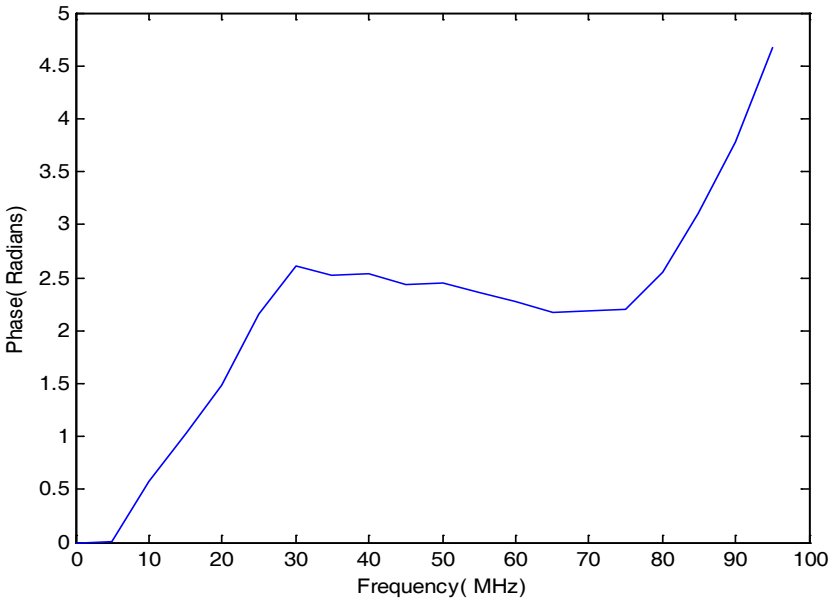

Figure (4.9) Relative phase response of the complex field generated by the nonlinear model and shifted with respect to the phase at fundamental frequency, i.e. 5 MHz corresponding to Fig. 4.6

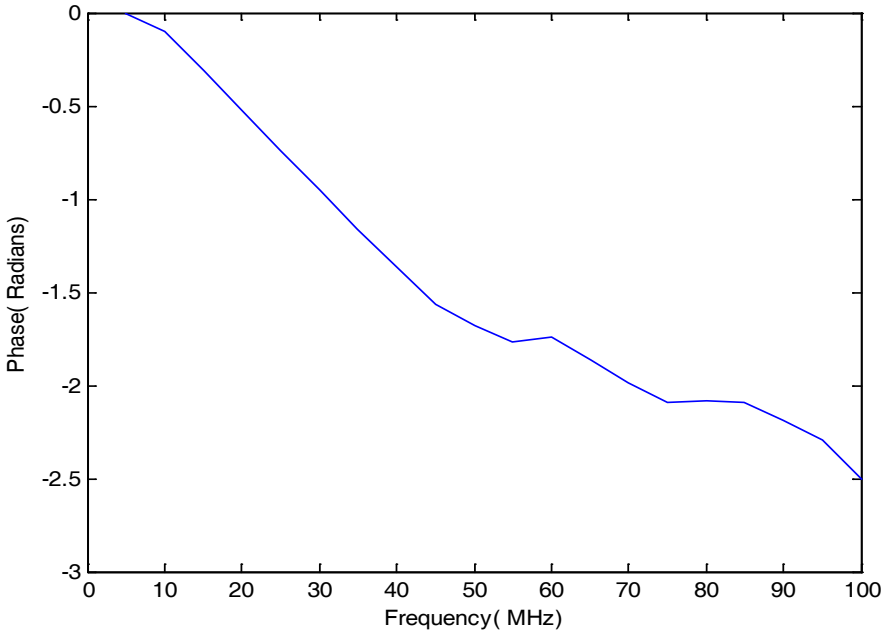

Figure (4.10) Relative phase response of the complex field measured by the Marconi hydrophone and shifted with respect to the phase at the fundamental frequency of the HIFU source; i.e. 5 MHz corresponding to Fig. 4.5

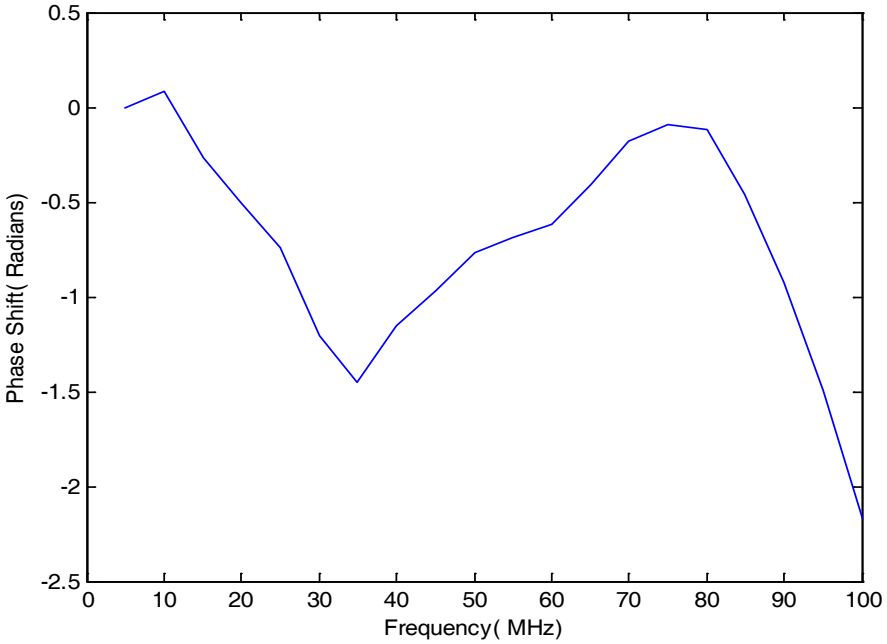

Figure (4.11) Final result of the Phase calibration for 50μm thick Marconi bilaminar membrane hydrophone, effective diameter - 500μm, cable length of 65 cm

The final phase shift, calculated after comparison of the nonlinear model and the experimentally determined relative phases obtained by using Eqs. (20)-(22), is shown in Fig. 4.11.

In the amplitude calibration result shown in Fig. 4.12, two resonances can be observed distinctly centered at around 20 MHz due to the thickness of the PVDF film used in the hydrophone, and 80 MHz observed due to the cable resonance [47].

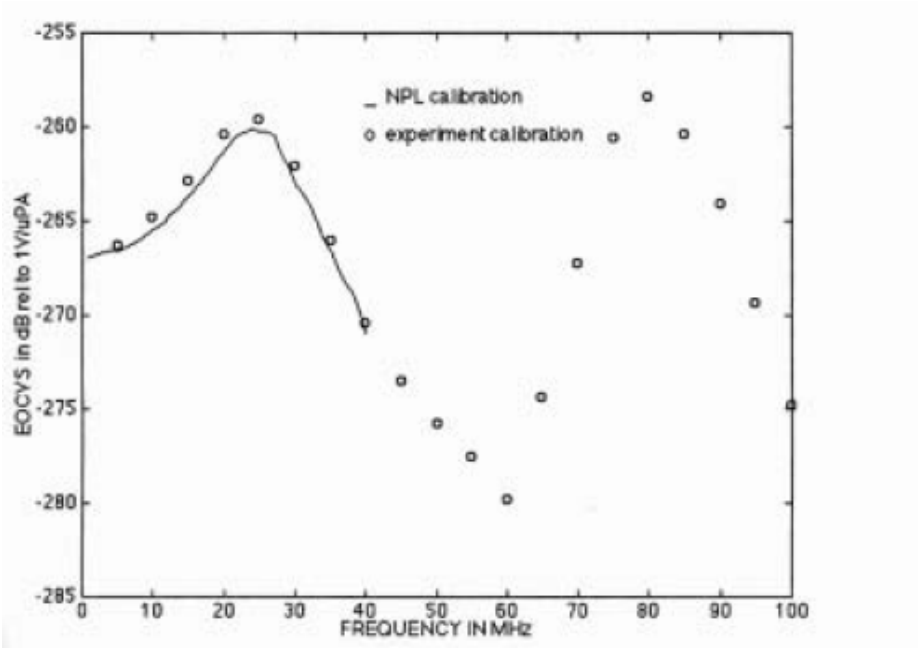

Figure (4.12) Amplitude Calibration of a similar Marconi hydrophone calculated by using nonlinear approach [47].

With respect to the phase response in Fig 4.11, the first steep slope occurs at around 20 MHz, which corresponds to the fundamental thickness mode resonance of the PVDF film used. Other two components to be observed here are the second thickness mode of the PVDF membrane, which can be observed at around 60 MHz frequency corresponding to a change in the slope, and the resonance due to the cable of length 65 cm connected to the hydrophone, at around 80 MHz. These resonating frequencies were also discussed previously [47] with respect to the amplitude response. These resonating frequencies also correspond to the values observed by Cooling et al [31], who also used hydrophone of corresponding PVDF film and cable length.

No reference phase response for the membrane hydrophones used in the study was available and hence commercially available PiezoCAD software (Sonic Concepts,

Woodinville, WA); was used to predict the amplitude and the phase response of a bilayered membrane hydrophone for conditions similar to those used for the experiments. Specifically, the relative phase response of the model was unwrapped manually by inversing the phases corresponding to values greater than π where the software had introduced jumps of 2π, and eliminating the jumps of π which the software introduced at the amplitude's zeroes. The result obtained is given in Fig. 4.13.

To further validate the theory and the measurement approach, another membrane hydrophone was tested using a different HIFU source operating at a fundamental frequency of 10 MHz. The HIFU source [46] was excited with 10 cycles tone burst and at an excitation level of 150 Vpp. The hydrophone used was a Precision Acoustics membrane which was custom made for operations in the frequency range up to 100 MHz and above, with an effective sensitive diameter of 400μm with a preamplifier. Fig. 4.14 depicts the voltage time waveform measured by the second membrane hydrophone.

This pressure-time signal was FFT'ed and its amplitude and phase responses are given in Figs. 4.15 and 4.16 respectively. Only 10 cycles were taken into consideration for the FFT in order to minimize the noise observed in the frequency domain.

The corresponding amplitude and the relative phase responses obtained using the nonlinear JW model are given in Figs. 4.17 and 4.18 respectively. The relative phase was again calculated following the protocol discussed in Chapter 3.

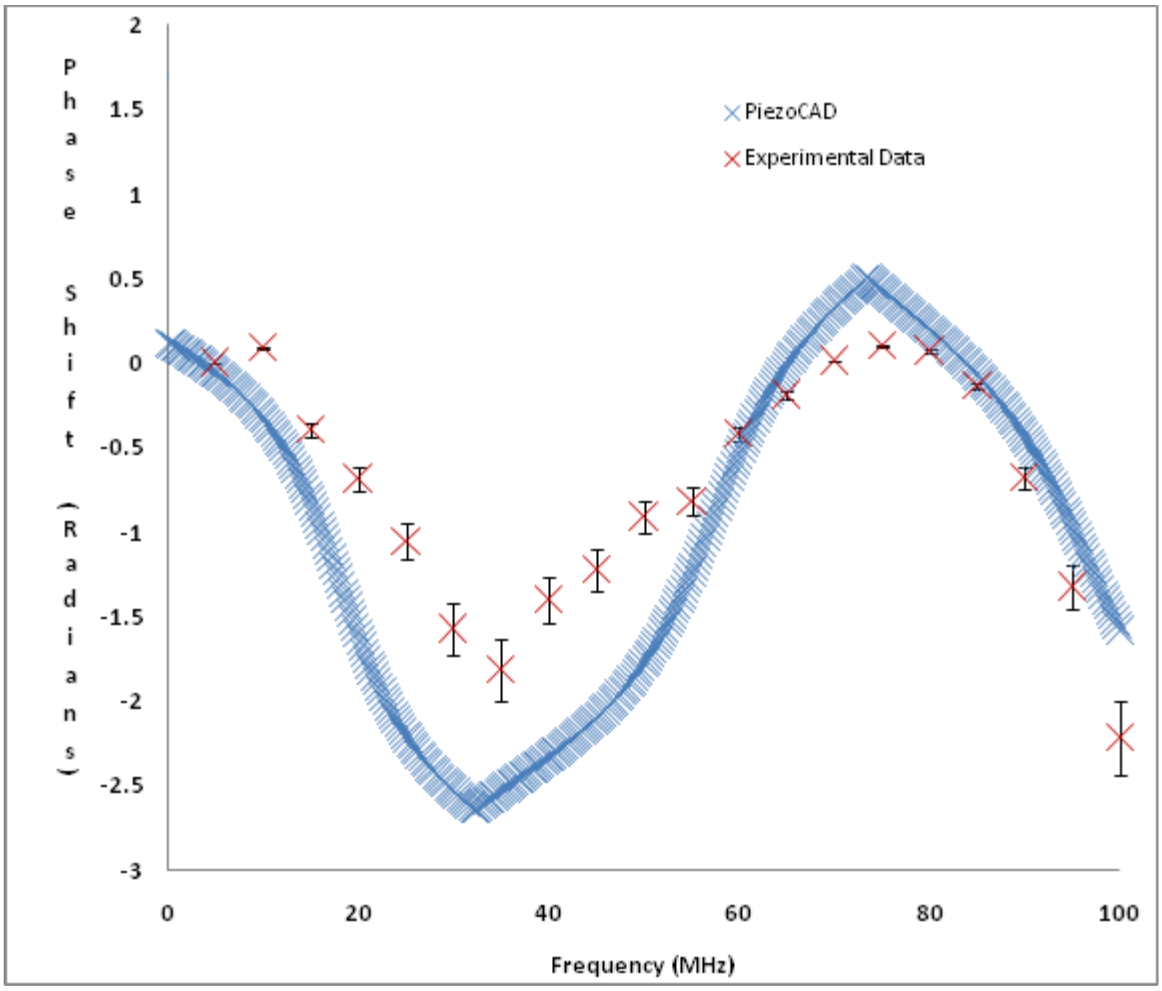

Figure (4.13) Final phase shift for 500μm effective diameter Marconi hydrophone with 50μm thick PVDF membrane and terminated by a 65 cm coaxial cable is given by red crosses, and the PiezoCAD relative phase results are given by blue crosses. Pressure-time waveform is generated by a 1.52 MHz HIFU source operating at 5 MHz. The calibration is based on the result predicted by JW model (see Chapter 2)

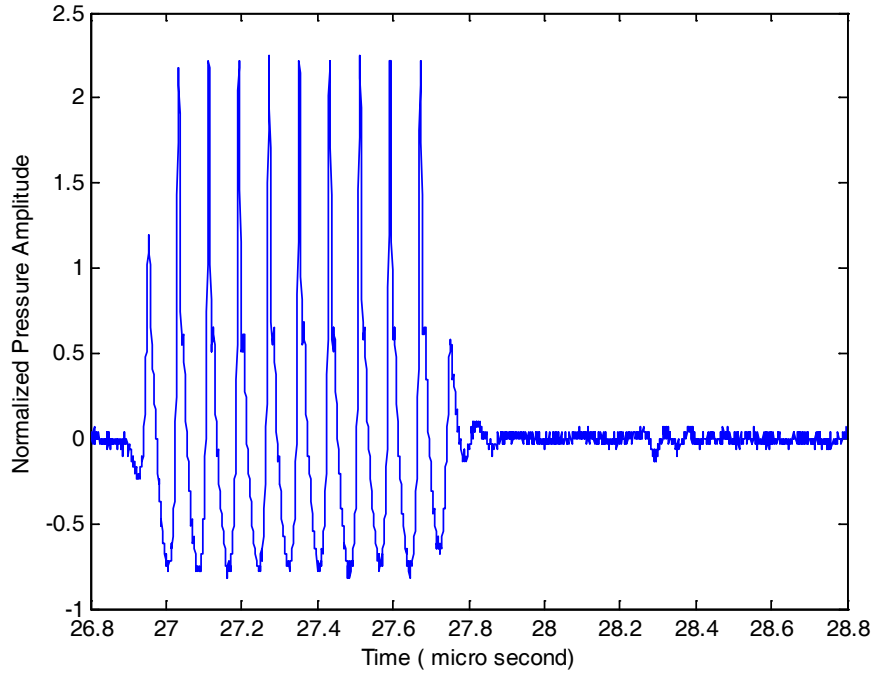

Figure (4.14) Pressure-time waveform measured by Precision Acoustics membrane hydrophone with an effective diameter of 400μm, 10 cycles and generated by a 10 MHz frequency HIFU source excited by a 10 cycle pulse of 150 Vpp level.

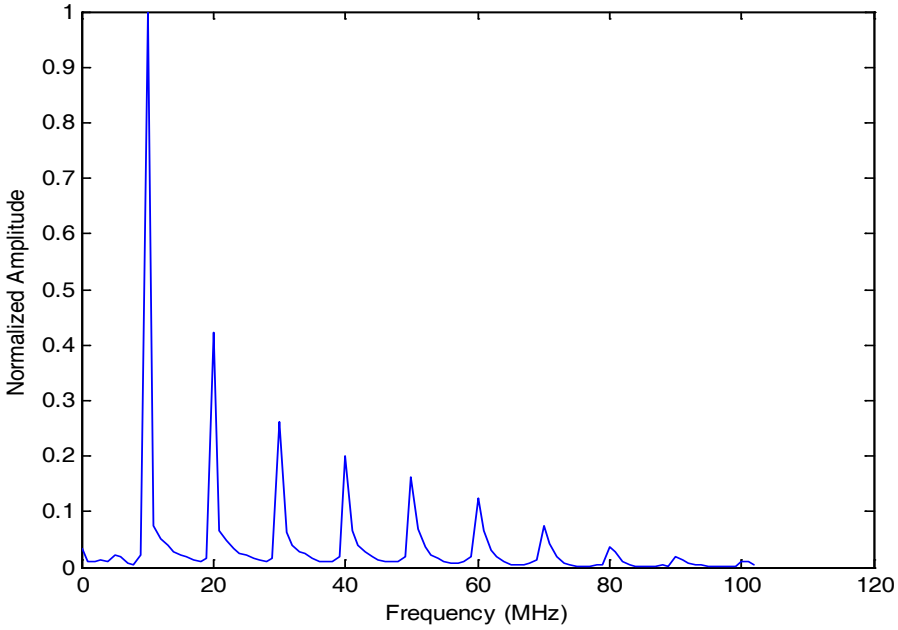

Figure (4.15) Normalized amplitude response of the pressure-time waveform depicted in Fig. 4.14

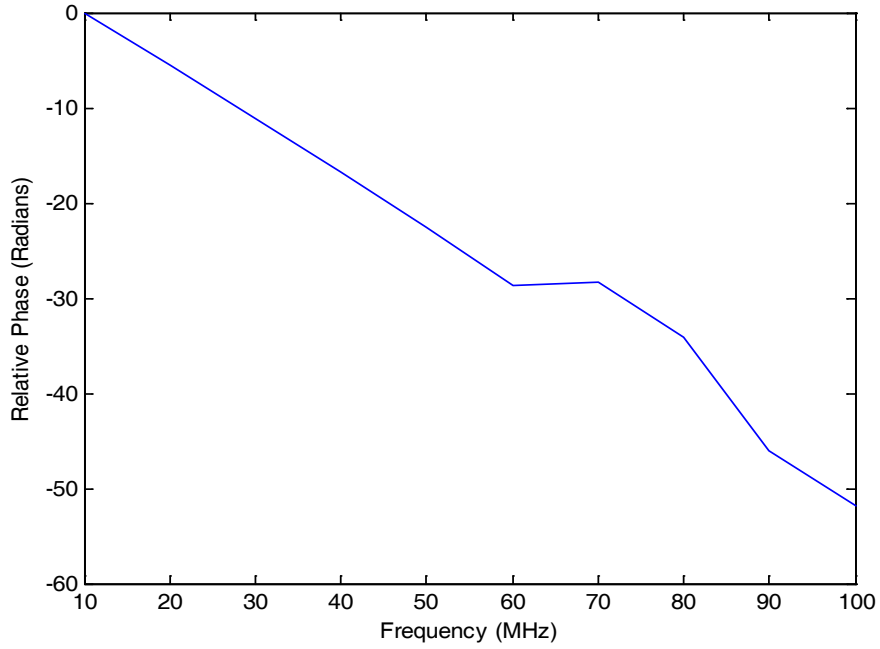

Figure (4.16) Relative phase response of the pressure-time waveform in Fig. 4.14

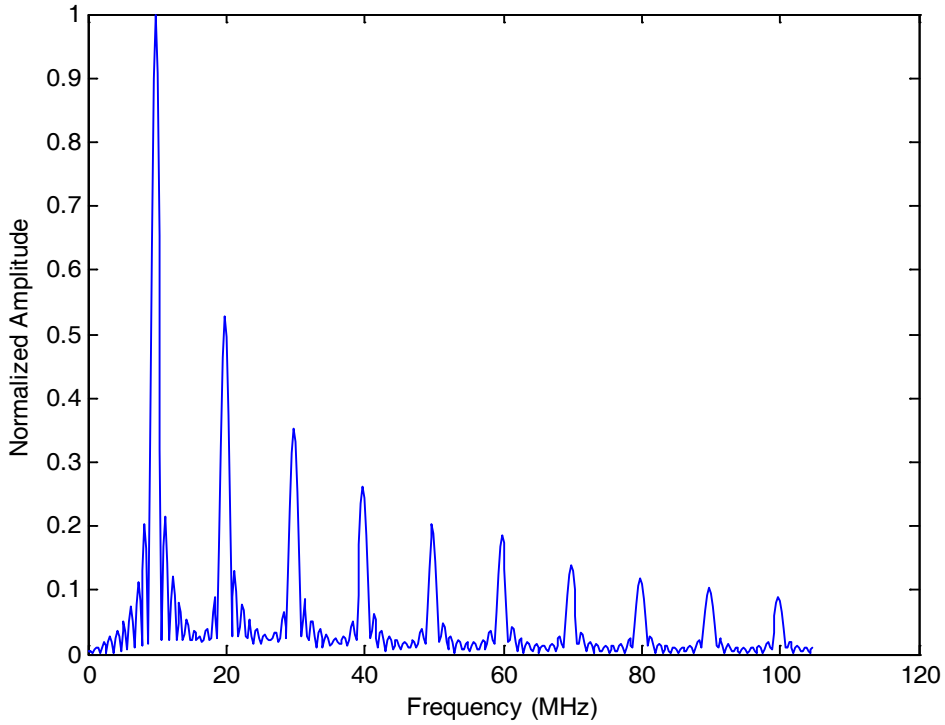

Figure (4.17) Normalized amplitude response of the complex field generated by the JW model for the 10 MHz HIFU source.

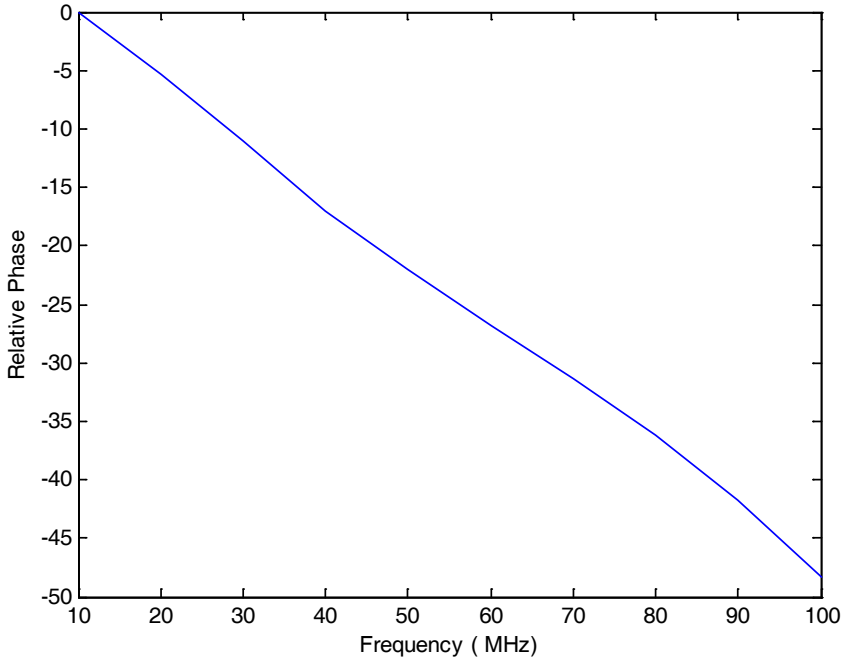

Figure (4.18) Relative phase simulated by JW model for the 10 MHz source.

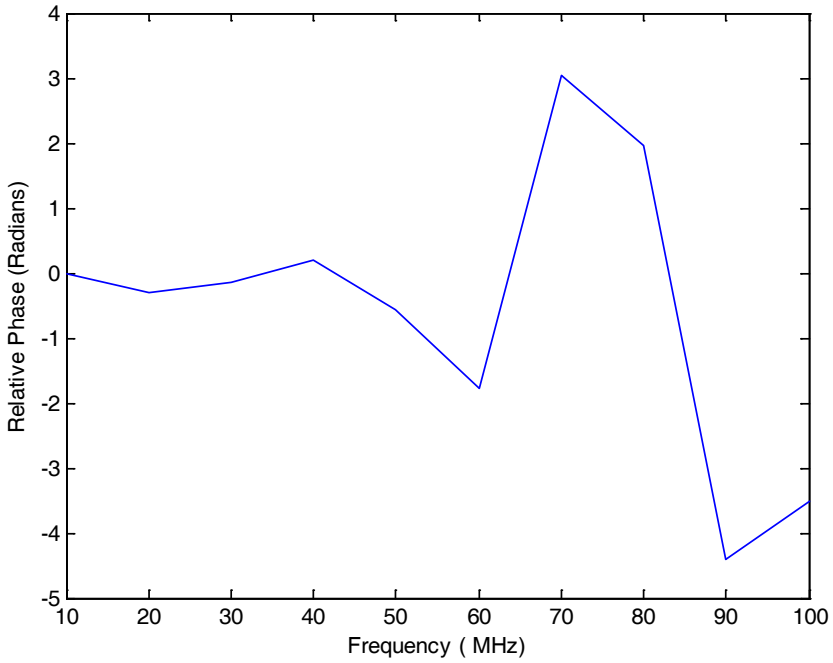

Figure (4.19) Final phase shift for 400μm effective diameter Precision Acoustics hydrophone terminated by a preamplifier, calculated using Eqs (22)-(24).

The final phase shift calculated by comparing the relative phases obtained by the JW model simulation and experimentally recorded by the 400µm Precision Acoustics bilayered membrane hydrophone in a nonlinear field generated by 10 MHz source is shown in Fig. 4.19.

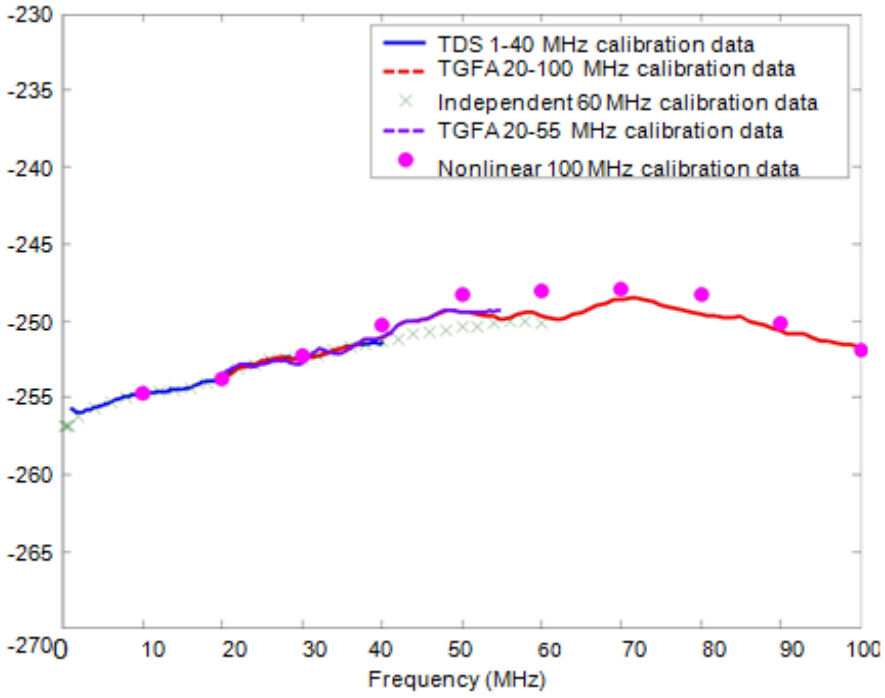

Figure (4.20) Amplitude calibration of the 400µm effective diameter Precision Acoustics membrane hydrophone terminated by a preamplifier [48].

The amplitude calibration of this membrane hydrophone is shown in Fig. 4.20 [48, 49]. The phase result obtained using the nonlinear approach is shown in Fig. 4.19 and it clearly corresponds to the resonances observed in Fig. 4.20. The thickness mode resonance of the Precision Acoustics membrane hydrophone occurs at a frequency of 70 MHz, which can be clearly seen in Figs. 4.19 and 4.20 corresponding to a phase shift of π and maximum amplitude sensitivity respectively.

Chapter: 5 – Discussion and Conclusions

The phase measurements performed with two different membrane hydrophones are shown in Figs. 4.13 and 4.19. Figure 4.13 depicts the total end-of-cable phase shift observed for the first membrane hydrophone used in experimental study. This hydrophone has an effective diameter of 500μm, 50μm thickness corresponding to the 1st membrane resonance at about 20 MHz and was terminated with 65 cm of coaxial cable. The amplitude response of the first membrane hydrophone is shown in Fig. 4.4, up to 40 MHz and up to 100 MHz in Fig. 48 of [47]. This information is reproduced in Fig. 4.12 to facilitate the analysis of the final result.

The phase calibration results were obtained by the nonlinear method discussed in Chapters 2 and 3. The experimentally determined relative phase is given in Fig. 4.10 and the nonlinear JW model predicted phase is shown in Fig. 4.9. No thickness or coaxial cable induced resonances were observed in the predicted phase response. The results shown in Fig. 4.9 are also consistent with the JW model predicting point receiver response. On the other hand, the experimentally determined amplitude response of the membrane hydrophone shown in Fig. 4.4 up to 40MHz and Fig. 4.12 with exactly the same coaxial cable length of 65 cm, exhibits the 1st resonance at 20 MHz. This agrees very well with $\frac{\lambda}{2}$ resonance of 50μm thickness of the PVDF material. The 2nd membrane resonance at 60 MHz as well as the 1st at 20 MHz is observed as maximum slope amplitude in the phase vs frequency plot in Fig. 4.11. The second thickness mode resonance of the hydrophone element corresponds to the $\frac{3\lambda}{2}$ frequency. For our first

membrane hydrophone this resonance appears to be suppressed by the resonance due to the cable length observed at 80 MHz. This resonance was reported to be in the vicinity of 70 MHz for a similar hydrophone terminated with coaxial cable of approximately the same in [11].

Very good agreement to within 20% in the frequency range up to 100 MHz, Fig. 4.8, between the amplitude response of the Marconi membrane hydrophone and that predicted by JW model was observed for our study.

The final phase shift plot, Fig. 4.13, also follows a similar resonance pattern, and the first rapid change in the slope appears at a frequency of around 20 MHz, which corresponds to the fundamental resonance frequency of the hydrophone used. As the impedance at the resonance is real, a phase shift of (n * π) radians should be observed; but the phase at the fundamental frequency observed was around 0.1 radians which further shifts the value of the phase observed at higher frequencies when calculated with respect to the fundamental. Hence we observed a phase of -0.75 radians at the resonance frequency of 20 MHz. But the phase shift value observed was close to zero radian at the 2^{nd} resonance at around 80 MHz for the first membrane hydrophone shown in Fig. 4.13. The phase shift observed in Fig. 4.13 also corresponds well with the values reported in [31], for both the fundamental frequency of 20 MHz and the cable induced resonances.

The results for the second PVDF hydrophone, which had an effective diameter of 400μm and a 2*9μm thickness corresponding to the 1^{st} resonance at about 70 MHz, and was terminated with a preamplifier are shown in Figs 4.16 and 4.19, and indicate a flat shift till 40 MHz and a resonance at around 70 MHz. This phase response agrees well with the

amplitude response of the same hydrophone reproduced here in Fig. 4.20. The phase value observed in Fig 4.19 at the resonance (70 MHz) was ~ π, which also corresponds to standard value of n* π observed at the resonances.

The agreement between the experimental results and the phase shift predicted by the nonlinear model used here confirms that the nonlinear approach as originally proposed in [31] is applicable to determine phase characteristics of "well behaved" (theoretically predictable) amplitude frequency response. As reported in [11, 47, 50], the cable length influences on the amplitude and the phase response for PVDF membrane hydrophones in the frequency domain were observed in the study. These reported responses could be further examined by varying the length of the terminating cable. Although this was not followed in this work due to the decreasing end-of-cable sensitivity and inadequate S/N ratio, availability of a more powerful HIFU source could facilitate such study. An increase in the length of the cable would shift the resonance frequency to lower values and would also affect the phase response.

As already mentioned, the fundamental limitations of the phase characterization are primarily twofold: in case of membrane hydrophone, they are dependent on determination of boundary conditions to be input to the nonlinear propagation model. In the case of other than well behaved membrane hydrophones the method tested here is inadequate due to intrinsic and unpredictable resonances (and associated phase shifts) such as those present in needle hydrophones. One possible solution is presented by fiber optic hydrophones such as those described in [27, 29, 30, 51]. Such fiber optic hydrophones can operate as point receivers in 100 MHz bandwidth and exhibit virtually uniform amplitude response and zero phase shifts. Hence, they are well suited to be used

as references, where the phase of the tested hydrophone signal would be directly compared with the signal measured by the fiber optic hydrophone.

The uncertainties in the system can play a major role in the usability of the phase information obtained by the nonlinear approach discussed in this dissertation and in the making of critical decisions for medical purposes based on the obtained results for the strict guidelines set forth by FDA. The uncertainties involved for focused source working at a fundamental frequency of 5 MHz had already been studied intensively and could be found in Chapter 14 of [41]. The systematic uncertainties at 95% confidence level were used and are presented for the above studies. Although many parameters were used to calculate the overall uncertainty of the system, the determination of HIFU source's effective radius provided the greatest error for all the harmonics observed. These uncertainties also lead to incorrect boundary conditions to the JW model. The irregularities in the determination of the sensitivity at the fundamental frequency, influences the correct pressure at the surface determination, which in the ideal case, should be the average of the pressure variations observed at the various surface points of the HIFU source.

References

[1] C. A. Patton, G. R. Harris, and R. A. Phillips, “Output Levels and Bioeffects Indexes from Diagnostic Ultrasound Exposure Data Reported to the Fda,” *IEEE Transactions on Ultrasonics Ferroelectrics and Frequency Control,* vol. 41, no. 3, pp. 353-359, May, 1994.

[2] *N. E. M. A. American Institute of Ultrasound in Medicine*, "*Acoustic output measurement standard for diagnostic ultrasound equipment*," 2004.

[3] FDA, "*Revised FDA 510(k) Information for Manufacturers Seeking Marketing Clearance of Diagnostic Ultrasound Systems and Transducers*," 2008.

[4] *N. E. M. A. American Institute of Ultrasound in Medicine*, "*Standard for Real-Time Display of Thermal and Mechanical Acoustic Output Indices on Diagnostic Ultrasound Equipment, Rev. 1*," 2004.

[5] P. S. B. H. K. W. Kim, K. A. Harasiewicz, H. K. Gahunia, K. P. H. Pritzker, F. S. Foster,, “Imaging of immature articular cartilage using ultrasound backscatter microscopy at 50 MHz,” *Journal of Orthopaedic Research,* vol. 13, no. 6, pp. 963-970, 1995.

[6] D. H. Turnbull, T. S. Bloomfield, H. S. Baldwin *et al.*, “Ultrasound backscatter microscope analysis of early mouse embryonic brain development,” *Proc Natl Acad Sci U S A,* vol. 92, no. 6, pp. 2239-43, Mar 14, 1995.

[7] D. E. Goertz, J. L. Yu, R. S. Kerbel *et al.*, “High-frequency 3-D color-flow imaging of the microcirculation,” *Ultrasound in Medicine and Biology,* vol. 29, no. 1, pp. 39-51, Jan, 2003.

[8] R. C. Preston, Livett, A. J. and Bacon, D. R., “Absolute calibration of hydrophones in the frequency range 0·5 MHz to 15 MHz,” *Proc. Inst. Acoustics,* vol. 6, no. 5, pp. 60–67, 1984.

[9] G. R. Harris, “Pressure Pulse Distortion by Hydrophones Due to Diminished Low-Frequency Response,” *Ieee Transactions on Ultrasonics Ferroelectrics and Frequency Control,* vol. 42, no. 6, pp. 989-992, Nov, 1995.

[10] H. J. Bleeker, and P. A. Lewin, “A novel method for determining calibration and behavior of PVDF ultrasonic hydrophone probes in the frequency range up to 100 MHz,” *IEEE Trans Ultrason Ferroelectr Freq Control,* vol. 47, no. 6, pp. 1354-62, 2000.

[11] D. R. Bacon, “Characteristics of a PVDF Membrane Hydrophone for Use in the Range 1-100 MHz,” *Sonics and Ultrasonics, IEEE Transactions on,* vol. 29, no. 1, pp. 18-25, 1982.

[12] D. R. Bacon, “*Nonlinear acoustics in ultrasound calibration and standard*,” in *In: Frontiers of Nonlinear Acoustics*, *Proc. of 12th ISNA*, Austin, 1990.

[13] A. C. Baker, and V. F. Humphrey, “Distortion and high-frequency generation due to nonlinear propagation of short ultrasonic pulses from a plane circular piston,” *The Journal of the Acoustical Society of America,* vol. 92, no. 3, pp. 1699-1705, 1992.

[14] P. A. Lewin, S. Umchid, A. Sutin *et al.*, “Beyond 40 MHz frontier: the future technologies for calibration and sensing of acoustic fields,” *Journal of Physics: Conference Series,* vol. 1, pp. 38-43, 2004.

[15] P. Lum, M. Greenstein, E. D. Verdonk *et al.*, “A 150-MHz-bandwidth membrane hydrophone for acoustic field... (cover story),” *Hewlett-Packard Journal,* vol. 49, no. 3, pp. 6, 1998.

[16] G. T. Clement, “Perspectives in clinical uses of high-intensity focused ultrasound,” *Ultrasonics,* vol. 42, no. 10, pp. 1087-93, Aug, 2004.

[17] I. H. Rivens, and G. R. t. Haar, “High intensity focused ultrasound calibration; status and challenges,” *Journal of Physics: Conference Series,* vol. 1, pp. 180-180, 2004.

[18] P. A. Lewin, “Quo vadis medical ultrasound?,” *Ultrasonics,* vol. 42, no. 1-9, pp. 1-7, 2004.

[19] C. Koch, and W. Molkenstruck, “Primary calibration of hydrophones with extended frequency range 1 to 70 MHz using optical interferometry,” *IEEE Trans Ultrason Ferroelectr Freq Control,* vol. 46, no. 5, pp. 1303-14, 1999.

[20] K. Brendel, “Calibration of ultrasonic probe transducers,” *The Journal of the Acoustical Society of America,* vol. 59, no. S1, pp. S27-S27, 1976.

[21] G. Ludwig, and K. Brendel, “Calibration of hydrophones based on reciprocity and time delay spectrometry,” *IEEE Trans Ultrason Ferroelectr Freq Control,* vol. 35, no. 2, pp. 168-74, 1988.

[22] P. Pesque, and C. Mequio, "A New and Fast Calibration Method for Ultrasonic Hydrophones." IEEE Ultrasonics Symposium, pp. 743-747.

[23] E. G. Radulescu, P. A. Lewin, J. Wojcik *et al.*, “Calibration of ultrasonic hydrophone probes up to 100 MHz using time gating frequency analysis and finite amplitude waves,” *Ultrasonics,* vol. 41, no. 4, pp. 247-54, Jun, 2003.

[24] D. R. Bacon, "A New Method for Ultrasonic Hydrophone Calibration," Ultrasonics Symposium, 1982, pp. 700-704.

[25] R. C. Chivers, “Time-delay spectrometry for ultrasonic transducer characterisation,” *Journal of Physics E: Scientific Instruments,* vol. 19, no. 10, pp. 834-843, 1986.

[26] P. C. Pederson, P. A. Lewin, and L. Bjorno, “Application of time-delay spectrometry for calibration of ultrasonic transducers,” *IEEE Trans Ultrason Ferroelectr Freq Control,* vol. 35, no. 2, pp. 185-205, 1988.

[27] C. Koch, “Amplitude and phase calibration of hydrophones by heterodyne and time-gated time-delay spectrometry,” *IEEE Trans Ultrason Ferroelectr Freq Control,* vol. 50, no. 3, pp. 344-8, Mar, 2003.

[28] P. Lum, M. Greenstein, C. Grossman *et al.*, “High-frequency membrane hydrophone,” *Ultrasonics, Ferroelectrics and Frequency Control, IEEE Transactions on,* vol. 43, no. 4, pp. 536-544, 1996.

[29] V. Wilkens, and C. Koch, “Amplitude and phase calibration of hydrophones up to 70 MHz using broadband pulse excitation and an optical reference hydrophone,” *The Journal of the Acoustical Society of America,* vol. 115, no. 6, pp. 2892-2903, 2004.

[30] P. A. Lewin, C. Mu, S. Umchid *et al.*, “Acousto-optic, point receiver hydrophone probe for operation up to 100 MHz,” *Ultrasonics,* vol. 43, no. 10, pp. 815-21, Dec, 2005.

[31] M. P. Cooling, and V. F. Humphrey, “A nonlinear propagation model-based phase calibration technique for membrane hydrophones,” *IEEE Trans Ultrason Ferroelectr Freq Control,* vol. 55, no. 1, pp. 84-93, Jan, 2008.

[32] F. A. Duck, “Nonlinear acoustics in diagnostic ultrasound,” *Ultrasound Med Biol,* vol. 28, no. 1, pp. 1-18, Jan, 2002.

[33] V. F. Humphrey, M. P. Cooling, T. M. Duncan *et al.*, "P2C-1 The Peak Rarefactional Pressure Generated by Medical Ultrasound Systems in Water and Tissue: A Numerical Study." pp. 1604-1607.

[34] K. J. Parker, and E. M. Friets, “On the measurement of shock waves,” *IEEE Trans Ultrason Ferroelectr Freq Control,* vol. 34, no. 4, pp. 454-60, 1987.

[35] Kinsler L.E, Coppens A.B, Sanders J.V, Frey A.R, "*Fundamentals of Acoustics*", Fourth ed, Chapter 4 - pp. 91-112, Chapter 16 - pp. 478-493, 2000.

[36] P. A. Lewin, “Miniature piezoelectric polymer ultrasonic hydrophone probes,” *Ultrasonics,* vol. 19, no. 5, pp. 213-216, 1981.

[37] A. S. DeReggi, S. C. Roth, J. M. Kenney *et al.*, "Piezoelectric polymer probe for ultrasonic applications," *The Journal of the Acoustical Society of America,* vol. 69, no. 3, pp. 853-859, 1981.

[38] G. R. Harris, "Sensitivity Considerations for PVDF Hydrophones Using the Spot-Poled Membrane Design," *Sonics and Ultrasonics, IEEE Transactions on,* vol. 29, no. 6, pp. 370-376, 1982.

[39] R. C. Preston, D. R. Bacon, A. J. Livett *et al.*, "PVDF membrane hydrophone performance properties and their relevance to the measurement of the acoustic output of medical ultrasonic equipment," *Journal of Physics E: Scientific Instruments,* vol. 16, no. 8, pp. 786-796, 1983.

[40] M. Platte, "*A polyvinylidene fluoride needle hydrophone for ultrasound applications*," *Ultrasonics,* vol. 23, pp. 113-118, 1985.

[41] M. C. Ziskin, P. A. Lewin, "Ultrasonic Exposimetry," Chapter 8-Mark E. Schafer-pp. 217-255, Chapter 14-Marvin C. Ziskin-pp. 409-443, *CRC Press, Boca Raton, Florida,1993.*

[42] D. G. Shombert, and G. R. Harris, "Use of Miniature Hydrophones to Determine Peak Intensities Typical of Medical Ultrasound Devices," *Ultrasonics, Ferroelectrics and Frequency Control, IEEE Transactions on,* vol. 33, no. 3, pp. 287-294, 1986.

[43] D. R. Bacon, "Finite amplitude distortion of the pulsed fields used in diagnostic ultrasound," *Ultrasound in Medicine & Biology,* vol. 10, no. 2, pp. 189-195, 1984.

[44] J. Wojcik, "Conservation of energy and absorption in acoustic fields for linear and nonlinear propagation," *The Journal of the Acoustical Society of America,* vol. 104, no. 5, pp. 2654-2663, 1998.

[45] E. G. Radulescu, J. Wojcik, P. A. Lewin *et al.*, "Nonlinear propagation model for ultrasound hydrophones calibration in the frequency range up to 100 MHz," *Ultrasonics,* vol. 41, no. 4, pp. 239-45, Jun, 2003.

[46] "http://www.sonicconcepts.com/."

[47] H. J. Bleeker, and Drexel University. School of Biomedical Engineering Science and Health Systems., "A new method of hydrophone calibration using the KZK time domain finite difference algorithm," Thesis (Ph D), Drexel University, 1998., 1998.

[48] S. Umchid, P. A. Lewin, and Drexel University. School of Biomedical Engineering & Science., "Development of calibration techniques for ultrasonic hydrophone probes in the frequency range from 1 to 100 MHz," Thesis (Ph D),Drexel University,Philadelphia, Pa., 2007.

[49] S. Umchid, R. Gopinath, K. Srinivasan *et al.*, "Development of calibration techniques for ultrasonic hydrophone probes in the frequency range from 1 to 100 MHz," *Ultrasonics,* vol. 49, no. 3, pp. 306-11, Mar, 2009.

[50] P. N. Gélat, R. C. Preston, and A. Hurrell, "A theoretical model describing the transfer characteristics of a membrane hydrophone and validation," *Ultrasonics,* vol. 43, no. 5, pp. 331-341, 2005.

[51] J. Staudenraus, and W. Eisenmenger, "Fibre-optic probe hydrophone for ultrasonic and shock-wave measurements in water," *Ultrasonics,* vol. 31, no. 4, pp. 267-273, 1993.

APPENDIX I

Hydrophone

Instrument	Serial Number	Type	Dimensions	Manufacturer
Marconi Hydrophone	ER 208	Bilaminar Membrane	500µm Dia, 2*25µm thick PVDF	Marconi (no longer available)
Precision Hydrophone	PA-UC-099	Bilaminar Membrane	400µm Dia, 2*9µm thick PVDF	Precision Acoustics (Custom Made)
Needle Hydrophones	NTR 07050589, MI 583	Needle	500µm Dia, 25 µm Thick PVDF	NTR, Force Institute.
Sonora Hydrophone	S5-165	Bilaminar Membrane	400µm	Sonora Medical

Transducer

Focal Number	Frequency	Manufacturer
Focal Number 4.21	Central Frequency = 10 MHz	Olympus/Panametrics
Focal Number 1.9	Central Frequency = 1.5 MHz Third Harmonic Frequency = 5 MHz	Sonic Concepts

Equipments

Equipment	Manufacturer	Model	Specifications
Function Generator	Agilent	33250A	80 MHz Function/Arbitrary Waveform Generator
Power Amplifier	ENI	3100LA	250 KHz – 150 MHz Gain 55dB
Digital Oscilloscope	Tektronix	TDS2022	200 MHz Bandwidth,2GS/s Sample Rate

APPENDIX II: Assessment of overall uncertainty of hydrophone calibration system

The uncertainties involved with the acoustic calibration system were calculated to be at 95% confident level [41] after several repeated measurements. The random uncertainty, U_r, at 95% confident level was calculated by the equation:

$$U_r = t_{0.95} * \frac{Sx}{\sqrt{n}}$$

Where *t* was the student's t factor, *Sx* is the standard deviation of the samples, n was the number of samples. The systematic uncertainty, U_s, was calculated based on the known uncertainties like, harmonic distortion of the power amplifier, function generator errors, alignment inaccuracies, issues with the linear performance of the HIFU source, oscilloscope, and other minor issues concerning the noise floor, ground vibrations and others causes of uncertainty. The overall uncertainty of the system was calculated by the quadratic sum of the random and the systematic uncertainties, and defined by the equation below.

$$U_T = \sqrt{U_r^2 + U_s^2}$$